

Newtonian nudging for a Richards equation-based distributed model

M. Verbunt* and C. Paniconi

Technical Report

*Center for Advanced Studies, Research and Development in Sardinia (CRS4)
Cagliari, Italy*

** SOCRATES student visiting from Wageningen University
Wageningen, The Netherlands*

November, 2001

Contents

| | | |
|----------|--|-----------|
| 1 | Summary | 7 |
| 2 | Introduction | 8 |
| 3 | The CATHY model | 9 |
| 3.1 | Overview | 9 |
| 3.2 | The subsurface flow module | 10 |
| 3.3 | The surface routing module | 12 |
| 3.4 | Topographic depressions | 13 |
| 3.5 | Coupling of the surface and subsurface flow module | 13 |
| 4 | Data assimilation | 14 |
| 4.1 | Overview | 14 |
| 4.2 | The Newtonian relaxation method | 15 |
| 4.3 | Nudging in the CATHY model | 16 |
| 5 | Application of the CATHY model | 19 |
| 5.1 | Introduction | 19 |
| 5.2 | The atmospheric perturbation run | 20 |
| 5.2.1 | The influence of the nudging technique on the timestep size | 20 |
| 5.2.2 | The influence of the nudging technique on the hydrological results | 21 |
| 5.3 | The initial conditions perturbation run | 27 |
| 5.3.1 | The influence of the nudging technique on the timestep size | 27 |
| 5.3.2 | The influence of the nudging technique on the hydrological results | 28 |
| 6 | The influence of the nudging parameters | 32 |
| 6.1 | Introduction | 32 |
| 6.2 | The influence of G | 32 |
| 6.3 | The influence of R_{xy} | 37 |

| | | |
|----------|--|-----------|
| 6.4 | The influence of τ | 41 |
| 7 | Conclusions and recommendations | 44 |
| 7.1 | Conclusions | 44 |
| 7.2 | Recommendations | 46 |
| | References | 46 |

List of Figures

| | | |
|----|---|----|
| 1 | Atmospheric forcing, boundary conditions and runoff generation in the CATHY model (after <i>Putti and Paniconi [2001 in preparation]</i>). | 11 |
| 2 | The test case used in this study representing a small catchment with an internal lake. 50 × 50 meter DEM surface cell elevations (left) and surface flow paths (right). | 13 |
| 3 | The horizontal, vertical, and temporal dependency of the 4-dimensional weighting functions. | 18 |
| 4 | The temporal variation of the timestep size of the nudging and no nudging run for the atmospheric perturbation run. | 21 |
| 5 | The histogram of timestep size for the nudging (left) and no nudging (right) run for the atmospheric perturbation run | 22 |
| 6 | The water table depths for the base run (top four plots), the nudging run (central four plots) and the no nudging run (bottom four plots) for the atmospheric perturbation run at four different times: $t = 0$, $t = 3600$, $t = 10800$ and $t = 14400$ seconds (from left to right). | 23 |
| 7 | The difference in water saturation at the surface nodes between the base run and the no nudging run (top three graphs) and between the base run and the nudging run (bottom three graphs) at three different times (3600, 10800 and 14400 seconds) for the atmospheric conditions perturbation run | 24 |
| 8 | The temporal variation of soil moisture at the five observation points for the base run (dotted line), no nudge run (dashed line) and the nudge run (solid line) performed by the atmospheric perturbation run with the two observation times at 3600 s and 10800 s. The nudging parameter values used are: $G=0.1$, $\epsilon = 1$, $\tau = 1800s$, $R_{xy} = 100$ m, and $R_z = 2$ m. Note that τ in the figures should have been 2τ | 26 |
| 9 | The temporal variation of the timestep size for the initial conditions perturbation run. | 27 |
| 10 | The histogram of timestep size for the nudging (left) and no nudging (right) run for the initial conditions perturbation run | 28 |
| 11 | The water table depths for the base run (top four plots), the nudging run (central four plots) and the no nudging run (bottom four) for the initial conditions perturbation run at 4 different times: $t = 0$, $t = 3600$, $t = 10800$ and $t = 14400$ seconds (from left to right). | 29 |
| 12 | The difference in water saturation at the surface nodes between the base run and the no nudging run (top four graphs) and between the base run and the nudging run (bottom four plots) for the initial conditions perturbation run at four different times: $t = 0$, $t = 3600$, $t = 10800$ and $t = 14400$ seconds (from left to right). | 30 |

| | | |
|----|---|----|
| 13 | The temporal variation of soil moisture at the five observation points for the base run (dotted line), no nudge run (dashed line) and the nudge run (solid line) performed by the initial condition perturbation run with the two observation times at 3600 s and 10800 s. The nudging parameter values used are: $G=0.1$, $\epsilon = 1$, $\tau = 1800s$, $R_{xy} = 100$ m, and $R_z = 2$ m | 31 |
| 14 | The influence of G on the temporal behavior of the soil moisture content at the five nudging points together with the base run (thick line) and the no nudging run (dotted line). 1: $G = 10^{-4}$, 2: $G = 10^{-3}$, 3: $G = 0.005$ 4: $G = 0.01$, 5: $G = 0.1$, 6: $G = 0.5$ | 36 |
| 15 | The influence of high G -values on the temporal behavior of the soil moisture content at two nudging points 1: $G = 0.1$, 2: $G = 1$, 3: $G = 10$ | 37 |
| 16 | The influence of R_{xy} on the spatial distribution of the difference between the base and nudging run. The upper three graphs show the results at the times (from left to right) 3600, 10800 and 14400 for $R_{xy} = 50$ m, the three plots in the center for $R_{xy} = 150$ m and the bottom three graphs for $R_{xy} = 250$ m. . | 39 |
| 17 | The influence of τ on the temporal behavior of the soil moisture content at the five nudging points together with the base run (thick line) and the no nudging run (dotted line). 1: $\tau = 900s$, 2: $\tau = 1350s$, 3: $\tau = 1800s$, 4: $\tau = 2250s$, 5: $\tau = 2700s$ | 43 |

List of Tables

| | | |
|----|--|----|
| 1 | Model parameter values for the test case. | 20 |
| 2 | The effect of the different G-values on the numerical and computational results. Note that “Total timesteps” does not include back-stepping occurrences. | 33 |
| 3 | The influence of G on the mean spatial difference of the soil moisture at the surface nodes between the base run and the nudging run at three different times for the atmospheric perturbation run. | 34 |
| 4 | The influence of G on the variance (σ) of the differences between the base- and nudging run of the spatial soil moisture values at the surface nodes averaged over the whole simulation time. | 35 |
| 5 | The effect of the different R_{xy} -values on the numerical and computational results. | 38 |
| 6 | The influence of R_{xy} on the mean spatial difference of the soil moisture at the surface nodes between the base run and the nudging run at three different times for the atmospheric perturbation run. | 38 |
| 7 | The influence of R_{xy} on the variance (σ) of the differences between the base- and nudging run of the spatial soil moisture values at the surface nodes averaged over the whole simulation time. | 40 |
| 8 | The effect of the different τ -values on the numerical and computational results. | 41 |
| 9 | The influence of τ on the mean spatial difference of the soil moisture at the surface nodes between the base run and the nudging run at three different times (4200 s, 7200 s, 14400 s) for the atmospheric perturbation run. | 42 |
| 10 | The influence of τ on the variance (σ) of the differences between the base- and nudging run of the spatial soil moisture values at the surface nodes averaged over the whole simulation time. | 42 |

1 Summary

This report describes a series of simulations conducted with a hydrological model, CATHY, to test a recently implemented data assimilation technique, Newtonian nudging.

The data assimilation technique has been implemented in the spatially distributed CATHY (CATchment HYdrology) model to improve the hydrological results. The nudging data assimilation technique implemented is a relatively simple 4-D data assimilation technique in which the variables are driven (nudged) toward observation data by adding a physical forcing term (F), which is proportional to the difference between the actual solutions and the observations to be assimilated, to the model equation. In the CATHY model these terms have been added to the Richards equation.

The CATHY model has been applied to a test area of 300 by 550 meters, in order to test the nudging technique. This area is divided into 6 by 11 grid cells of 50 by 50 meters and contains a lake. In this application a four-hour evaporation perturbed and a four hour initial conditions perturbed run are made in order to investigate the effect of the nudging technique.

To obtain observation data a base run has been made, which is perturbed to differentiate the base run from the nudging and no nudging run. Both an atmospheric perturbation as well as an initial conditions perturbation run are made. From five different nodes (the nudging points), the obtained values of the base run are extracted and used as observation data during the defined assimilation times. In this four-hour simulation two assimilation periods are defined with observation times at respectively 1 and 3 hours and a nudging influence which lasts from half an hour before till half an hour after these observation times.

The results of the atmospheric perturbation run show that the nudging run is more efficient by requiring less timesteps for the simulation. The hydrological results for the nudging run are in better agreement with the observation data compared to the no nudging run. The water table depths around the nudging points are corrected toward the observed values and also the difference in soil moisture values at the surface nodes between the observed and computed data is much smaller for the nudging run than for the no nudging run. These improvements can especially be seen at and around the five nudging points. The mean areal decrease in computed error in surface soil moisture for the nudging run compared to the no nudging run is 35 percent at the two observation times and 29 percent at the end of the simulation.

Also the temporal distribution of the soil moisture at the five nudging points shows for the nudging run during the assimilation times a much better agreement with the observed values. The initial conditions perturbation run shows the same effect of the nudging technique on the hydrological results, however for this run the nudging run is less computationally efficient than the no nudging run.

For the atmospheric perturbation run the influence of some nudging parameters on the nudging effect has been investigated in order to get a better understanding of the nudging technique. The influence of three nudging parameters has been investigated; (i) the G -term, which determines the relative strength of the nudging term with respect to the physical forcing term, (ii) R_{xy} , which is the horizontal radius of influence of the nudging technique and (iii) τ , which is the half period of the defined time of nudging influence.

The results show that the convergence of the soil moisture values towards the observed values at the nudging points strongly varies for different values of G and τ , however for G values of 0.3 and higher no difference in convergence can be noticed. The computed mean areal error in surface soil moisture values generally decreases with increasing values of R_{xy} and G , however this decrease stabilizes for G -values larger than 0.1. The influence of τ on this mean areal error depends on whether the time, at which the error is determined, is located close or far away from the observation time. The influence of these three nudging parameters on the numerical and computational results has also been investigated. These results show for increasing G values an increasing number of back-stepping occurrences and therefore a larger CPU, while this CPU remains constant for increasing R values.

2 Introduction

Spatially distributed hydrological models are becoming more and more a necessity to get a complete understanding of the hydrological behavior at the catchment scale. The requested information for authorities needs to be more complete and detailed nowadays and for this a continued progress in the understanding of the hydrological catchment response is required. Distributed hydrological models are able to include the spatial distribution of boundary conditions and various input data such as rainfall, precipitation, land cover, soil characteristics and topography. Further they produce spatially distributed detailed outputs of hydrological properties and processes. The availability of remote sensing data, from which useful hydrological data can be extracted, makes the use of spatially distributed hydrological models more popular and more effective.

However one of the major problems facing spatially distributed modelling is the adjustment of spatial distributed model parameters. The data which are available to initialize, parameterize and calibrate the models often mismatch the model complexity and both models and observation data contain errors and uncertainties. With the availability of new data sources for hydrological process observations some of these problems can be alleviated. More availability and accessibility of detailed spatially distributed data makes it possible to introduce data assimilation techniques into the hydrological models [Marrocu and Paniconi 2001]. Data assimilation can be described as a generalization of objective analyses and the objective of data assimilation is to provide physically consistent estimates of spatially distributed environmental variables [McLaughlin 1995]. This is done, in the case of the Newtonian relaxation (or nudging) algorithm used in this study, by adding an additional forcing term to the model equation, which corrects the model results towards the observation data.

A problem applying data assimilation to hydrological models may be the incomplete knowledge of the spatial and temporal variability of hydrological variables and processes. Therefore it is required to have an adequate characterization of the temporal and spatial variability in the measurement equations and or interpolation and extrapolation formulas which are commonly used in data assimilation techniques. However due to parameterization and computational time most models using data assimilation techniques are not yet applicable at large catchment scales at this moment. On the other hand with the improvements in model and data quality arising from data assimilation and other advances, progress can be expected in turn in the understanding of the dynamics and interactions responsible for the spatial patterns we observe in runoff, water table levels and other components of the catchment scale water balance and, at larger scales, for the generation and persistence of floods, droughts, etc on

seasonal and interannual bases [*Paniconi et al.* 2001 in preparation].

Chapter 3 of this report will describe the CATHY model and its modules. Data assimilation, the Newtonian relaxation method and the nudging in the CATHY model are described in Chapter 4. The results of the application of the model including the nudging technique to a test case can be found in Chapter 5. The effect of the nudging parameters on the results is described in Chapter 6 and the last chapter summarizes the conclusions of this research and and some recommendations for future research.

3 The CATHY model

3.1 Overview

The CATHY (CATchment HYdrological) model is a physically-based distributed model for overland and subsurface flow simulation at the catchment scale [*Putti and Paniconi* 2001 in preparation]. The model couples a three-dimensional Richard's equation-based finite element subsurface flow module with a one-dimensional DEM-based finite difference surface routing module. The surface routing module, SURF-ROUTE [*Orlandini and Rosso* 1996] uses a diffusion-wave formulation for describing both the hillslope and channel flow. To account for the retardation and storage effects, the accumulation of water in depressions and lakes has been implemented. The subsurface module, FLOW3D [*Paniconi and Wood* 1993], is based on the solution of the Richard's equation for variably saturated porous media and describes the infiltration to and exfiltration from the vadose zone. The FLOW3D module partitions the atmospheric input (precipitation and evapotranspiration) into subsurface and surface flow. Starting from a digital elevation model discretization of the catchment surface and a corresponding three-dimensional grid of the underlying aquifer, the physical conditions at the surface and the soil properties are determined for each grid cell. Based on these properties, FLOW3D calculates then at each grid node the overland flux values, which are transferred to the DEM-cells and are implemented as sink or source terms in the SURF-ROUTE module. The SURF-ROUTE module routes these overland flux values and calculates the resulting ponding head values that will be used as a boundary condition in FLOW3D.

The mathematical model describing the subsurface and surface flow is based on the following partial differential equations [*Bixio et al.* 2000]:

$$\sigma(S_w) \frac{\partial \psi}{\partial t} = \nabla \cdot [K_s K_r(S_w) (\nabla \psi + \eta_z)] + q_s(h) \quad (1)$$

$$\frac{\partial Q}{\partial t} + c_k \frac{\partial Q}{\partial s} = D_h \frac{\partial^2 Q}{\partial s^2} + c_k q_L(h, \psi) \quad (2)$$

where $\sigma(S_w) = S_w S_s + \phi \frac{\partial S_w}{\partial \psi}$, $S_w(\psi)$ is the water saturation, S_s is the aquifer specific storage coefficient, ϕ is the porosity, ψ is the pressure head, t is the time, ∇ is the gradient operator, K_s is the saturated hydraulic conductivity tensor, $K_r(S_w)$ is the relative hydraulic conductivity function, $\eta_z = (0, 0, 1)^T$, z is the vertical coordinate directed upward and q_s represents distributed source (positive) or sink (negative) terms (volumetric flow rate per unit volume).

3.2 The subsurface flow module

The FLOW3D-module is a three-dimensional tetrahedral finite element model for flow in variably saturated porous media. It is based on the Richards equation and is applicable in both the saturated and the unsaturated zone and is able to handle temporally and spatially variable boundary conditions, including seepage faces and atmospheric inputs. The soil hydraulic properties are specified by K_s and by different characteristic relationships of $S_w(\psi)$ and $K_{rw}(\psi)$ such as those of *van Genuchten and Nielsen [1985]*, *Huyakorn et al. [1984]*, or *Brooks and Corey [1964]*. The ones of van Genuchten can be written as:

$$\theta(\psi) = \theta_r + (\theta_s - \theta_r)[1 + \beta]^{-\gamma}, \quad \psi < 0 \quad (3)$$

$$\theta(\psi) = \theta_s, \quad \psi \geq 0 \quad (4)$$

$$K_r(\psi) = (1 + \beta)^{-5\gamma/2} [(1 + \beta)^\gamma - \beta^\gamma]^2, \quad \psi < 0 \quad (5)$$

$$K_r(\psi) = 1, \quad \psi \geq 0 \quad (6)$$

where θ is the volumetric moisture content, θ_r is the residual moisture content, θ_s is the saturated moisture content (generally equal to the porosity ϕ), $\beta = (\psi/\psi_s)^n$, ψ_s is the capillary or air entry pressure head value, n is a constant, and $\gamma = 1 - 1/n$ for n approximately in the range $1.25 < n < 6$.

The corresponding general storage term is

$$\sigma = S_w S_s + \phi \frac{dS_w}{d\psi} \quad (7)$$

where $S_w = \theta/\theta_s$ and S_s is the specific storage.

The soil hydraulic characteristic equations used by *Huyakorn et al. [1984]* express the water saturation in terms of effective saturation S_e , in the form $S_w(\psi) = (1 - S_{wr})S_e(\psi) + S_{wr}$, where S_{wr} is the residual water saturation. The effective saturation-pressure head relation is then written as

$$\begin{aligned} S_e(\psi) &= [1 + \epsilon^n(\psi_a - \psi)^\eta]^{-\gamma} & \psi < \psi_a \\ S_e(\psi) &= 1 & \psi \geq \psi_a \end{aligned} \quad (8)$$

while two possible expressions for the relative conductivity-pressure head relationship are

$$k_{rw}(\psi) = k_{rw}(\psi) (S_e(\psi)) = S_e^\mu \quad (9)$$

and

$$k_{rw}(\psi) = 10^{G(S_e(\psi))} \quad (10)$$

where $G(S_e) \equiv aS_e^2 + (b - 2a)S_e + a - b$. In the above expressions ψ_a is the air entry pressure and $\epsilon, \eta, \gamma, \mu, a$, and b are constants.

The input flux values are considered as potential rainfall or evapotranspiration rates for the treatment of atmospheric boundary conditions while the actual rates, which depend on the

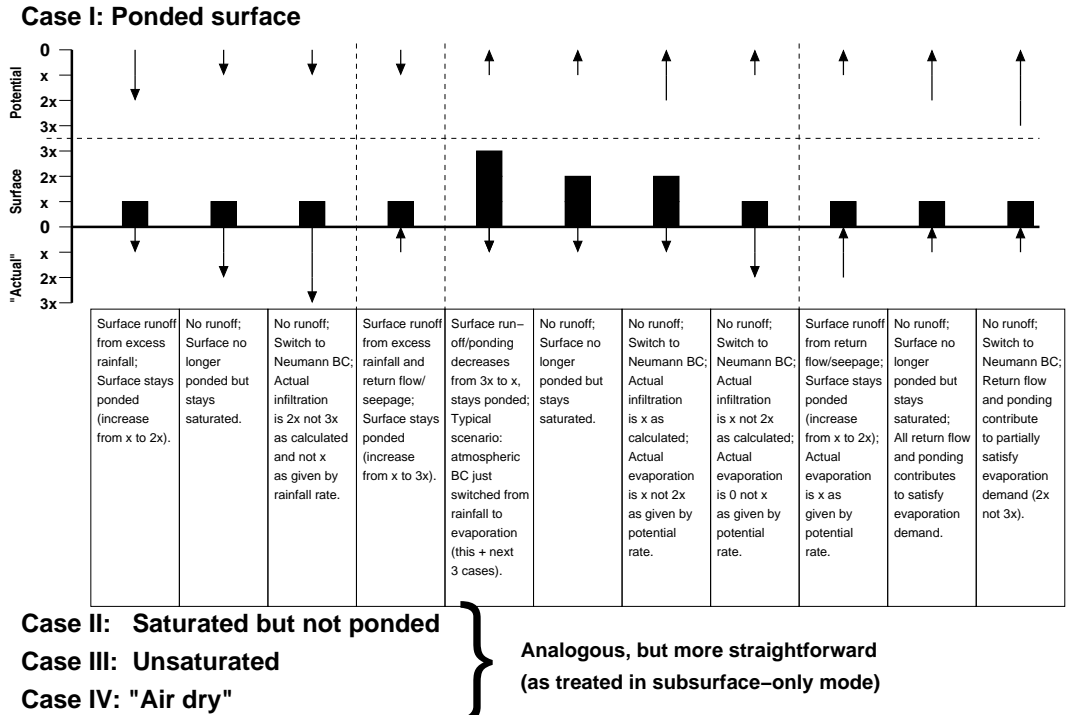


Figure 1: Atmospheric forcing, boundary conditions and runoff generation in the CATHY model (after Putti and Paniconi [2001 in preparation]).

prevailing pressure head and flux values at the surface, are calculated by the model during the simulation. Figure 1 shows the process of automatic switching of surface boundary conditions from a specified flux (Neumann) to a constant head (Dirichlet) condition, and vice versa, which has been implemented to correctly reproduce the physical phenomena occurring at the surface. A surface node can be in one of four states at any time:

- “air dry”,
- unsaturated,
- saturated (but not ponded)
- ponded.

Physically, the model input threshold pressure head parameter, pond-head-min, determines the distinction between a surface node being “saturated” or “ponded”. By introducing the boundary condition switching, which is performed by the subsurface module into the surface routing model, this module is extended to allow excess water to accumulate at the surface as ponding. This ponded water, converted to a flux q_L , constitutes a forcing term input to the routing model at each new time step. The treatment of the ponding case is schematized in Figure 1, which we subdivide into four scenarios of positive or negative potential and actual fluxes. For each scenario the figure explains what is the result (in terms of ponding, saturation status, runoff generation, boundary condition, and actual flux into or out of the soil) at the end of a time step if at the beginning of the time step the potential, actual, and ponding fluxes acting on a surface node during subsurface module execution are as indicated.

3.3 The surface routing module

In the CATHY model the catchment surface runoff is considered to be determined by the two processes of channel and hillslope transport operating across all the hillslope and stream channels forming a watershed and including storage and retardation effects of depressions and infiltration and exfiltration effects from subsurface soils. It is assumed that flow on hillslopes concentrates in rills caused by differences in soil erodibility or topographic irregularities. The rill formations are lumped at the DEM elemental scale into a single conceptual channel to reach a minimal computational effort and to economize on the number of model parameters. The drainage system network, consisting of these rills is extracted from the catchment DEM. The distinction between hillslope and channel flow is based on the “constant critical support area” concept as described by *Montgomery and Foufoula-Georgiou [1993]*. Channel flow is assumed to occur at all cells for which the upstream drainage area D equals or exceeds the threshold value D^* , while rill flow is assumed to occur at all those cells for which D does not exceeds the threshold value D^* .

A routing scheme developed on the basis of the Muskingum-Cunge method with variable parameters is used to describe both hillslope rill and network channel flows, with different distribution of the Gauckler-Strickler roughness coefficients to take into account the different processes that characterize the two physical phenomena [*Orlandini and Rosso 1996*]. Overland runoff is routed by the model from the uppermost catchment DEM cell downstream to the outlet, following the previously determined drainage network. The inflow or outflow rate q_L , which a grid cell will receive from an upslope neighbor cell and discharge to the downslope neighbor cell is given by:

$$q_l = \frac{q\Delta x\Delta y}{\Delta s} \quad (11)$$

where

q = the local contribution of surface runoff, as calculated by FLOW3D,

Δx and Δy are the cell sizes and

Δs = the channel length within the cell.

The convection diffusion flow equation, discretized by the Muskingum-Cunge method, is used to route the inflow hydrographs and the overland fluxes, q_L , into each individual channel. This equation is given by:

$$Q_{i+1}^{k+1} = C_1 Q_i^{k+1} + C_2 Q_i^k + C_3 Q_{i+1}^k + C_4 q_{L_{i+1}}^k \quad (12)$$

where Q_{i+1}^{k+1} is the discharge at the network location $(i+1)\Delta s$ and time $(k+1)\Delta t$, $q_{L_{i+1}}^k$ is the overland flow rate at the $(i+1)$ st space interval and time $k\Delta t$ and C_i is the routing coefficient which depends on c_k , on the channel length Δs , on the temporal interval Δt and on the numerical scheme. After the discharge in and out is determined, the water depth or ponding head h can be calculated for each cell from simple mass balance considerations.

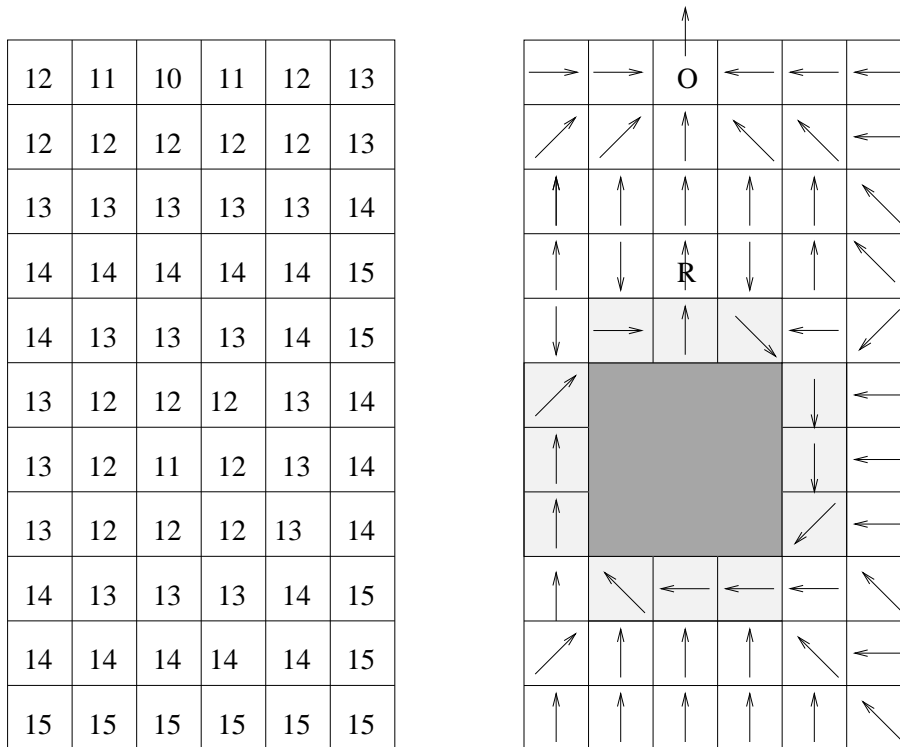


Figure 2: The test case used in this study representing a small catchment with an internal lake. 50×50 meter DEM surface cell elevations (left) and surface flow paths (right).

3.4 Topographic depressions

Isolated topographic depressions in the catchment DEM influence the formation of surface and subsurface flow fluxes and introduce inconsistent flow directions and when they represent actual lakes or ponds, they need to be properly handled in order to reproduce the storage and retardation effects on the catchment response. Figure 2 shows an example how topographic depressions are treated in the CATHY model.

Figure 2 shows the catchment DEM, used for the test case, on the left and on the right its schematized representation of the flow paths as calculated by the “depitching procedure”. The dark grey area in the middle represents the interior area of the depression and the buffer cells that force flow patterns are given in light grey. The output cell is marked with “O” while the reservoir cell is identified with “R”.

3.5 Coupling of the surface and subsurface flow module

The subsurface flow module, FLOW3D, and the surface flow module, SURF-ROUTE have been coupled to create a better representation of the hydrological catchment behavior. The coupling between the two modules is such that information regarding subsurface flow fluxes, ponding head values and nodal pressure head values can be exchanged between the two modules.

Equations (1) and (2) are solved using the assumption that the explicit in time nature of the Muskingum-Cunge discretization scheme allows the construction of the noniterative al-

gorithm:

for $t_k = 0$ to t_{max} with step Δt do:

- solve equation (2) using q_L^k as input to the SURF-ROUTE model, obtaining Q^{k+1} and from this the distribution of ponding heads h^{k+1} ;
- use h^{k+1} and precipitation/evapotranspiration input values at time t^{k+1} to set up boundary and initial conditions for FLOW3D, and solve equation (1) for ψ^{k+1}
- calculate, again with FLOW3D, the overland flux q_L^{k+1} using ψ^{k+1} and the balance between the atmospheric inputs and actual fluxes.

In this way the coupled modules determine for each time step and for each surface node whether it is ponded, saturated, below saturation or air dry, knowing for each of the surface nodes whether the potential atmospheric forcing is positive or negative. In the case of Dirichlet boundary condition the model knows whether the actual, back-calculated flux represents exfiltration or infiltration and its contributions to many hydrological components and it flags any anomalous events.

4 Data assimilation

4.1 Overview

Data assimilation can be described as a generalisation of objective analyses, whose main objective is to provide time dependent spatially distributed estimates that can be updated whenever new data become available. These estimates are derived from scattered observations at different times and locations supplemented by additional data that is available to force the estimation to the observed value. Data assimilation is most closely associated with and applied in the meteorological science since the early 1950's [Daley 1991]. However in the field of hydrology, data assimilation is still a relatively new phenomena and is not yet well established. In the last years data assimilation has been more and more introduced and applied to hydrological models. Some important data assimilation problems involve characterization of the spatial and temporal distribution of:

- Precipitation
- Evaporation
- Soil Moisture
- Water table elevation
- Solute concentration

In this study a relatively simple data assimilation method has been implemented in the complex spatially distributed CATHY model. The data assimilation technique used is Newtonian relaxation or nudging, in which model variables are driven (nudged) towards observations by an additional “forcing term” to the model equations [Houser *et al.* 1998]. This assimilation method will be explained in the next section.

4.2 The Newtonian relaxation method

The Newtonian relaxation method is a 4D data assimilation technique in which variables are driven toward observations by adding a forcing term to the model equation:

$$\frac{\partial s}{\partial t} = F(s) \quad (13)$$

This forcing term is proportional to the difference between the actual solutions and the observations to be assimilated. This term is added to the model equations for a certain period of time, the assimilation time (t_a), which contains in the center the observation time (t_0). After assimilation time is ended, the forcing term is relaxed and is not taken active anymore, causing that the model equations return to their original form. By adding the forcing term to the model equations this results in:

$$\frac{\partial s}{\partial t} = F(s) + GW(r, t)\epsilon(r)(s'_o - s) \quad (14)$$

where: s'_o are the observations interpolated to the model grid, G determines the relative strength of the nudging term with respect to the physical forcing term, $W(r, t)$ are weights to be specified and $\epsilon \leq 1$ is a factor measuring the accuracy of the observation that if we assume perfect measures should be taken equal to 1.

To get a better understanding of the Newtonian relaxation technique, consider a limited example which can be solved analytically and in which the following assumptions are made [*Marrocu and Paniconi 2001*]:

- the forcing terms of the system equations are zero,
- the product of the nudging factor and weighting function (GW) is a constant and
- $\epsilon = 1$

In this case a general solution of equation (14) is:

$$s(t) = s(t_0)e^{-GWt} + GW e^{-GWt} \int_0^{t_a} e^{GWt} s_0 \partial t \quad (15)$$

If in this case s_o is also assumed to be constant the solution of equation (14) is:

$$s(t) = s_o + e^{-GWt}(s(t_0) - s_o) \quad (16)$$

with $t_0 = t_o - t_a$ This equation shows that in the case of analyses factor $\epsilon = 1$, "nudged" solution reaches the observation state if assimilation time is infinite.

Because most measurements are taken at discrete points, the continuum form of the nudging equation needs to be discretized to be able to use these measurements. This can be done

by relaxing the system equation to individual scattered observations, which is done by interpolating the model grid values to the observation points r_i , then back to the model grid including this last step in the nudging term. In this case equation (14) becomes:

$$\frac{\partial s}{\partial t} = F(s) + G \frac{\sum_{i=1}^L W(r_i, t) \epsilon(r_i) (s'_o(r_i) - s(r_i))}{\sum_{i=1}^L W(r_i, t)} \quad (17)$$

4.3 Nudging in the CATHY model

The coupled distributed CATHY model is based on the Richards, the diffusion wave and the Darcy equations, which are widely known and accepted mathematical representations of verifiable conservation principles and therefore this model is a good candidate for implementing data assimilation. Due to computational complexity the model has only been applied to sub-catchment scale. Therefore is also chosen to implement this relatively simple data assimilation method because complicated and extended data assimilation techniques will only compound this problem. Another reason for choosing the nudging method is that this technique is able to conduct some initial investigations into the applicability and effectiveness of data assimilation for Richards equation-based 3D hydrological models.

The nudging term has been introduced into the Richard's equation which results in [*Paniconi et al.* 2001 in preparation]:

$$\sigma \frac{\partial \psi}{\partial t} = \nabla [K_s K_r (\nabla \psi + \eta_z)] + q + G \frac{\sum_{k=1}^{N_T} \sum_{i=1}^{N_X} W_{ki}^2(X, t) \epsilon_i (\theta_0 - \theta_i(t))}{\sum_{k=1}^{N_T} \sum_{i=1}^{N_X} W_{ki}(X, t)} \quad (18)$$

where N_T is the number of observation times, N_X is the number of observation points, θ_0 are the soil moisture observations, G determines the relative strength of the nudging term with respect to the model forcing term, $\epsilon \leq 1$ is a quality factor for the observation data and $W(X, t)$ are the 4-dimensional weighting functions which are assumed to be horizontally, vertically and temporally dependent and can be written as (Figure 3):

$$W(X, t) = W(d)W(z)W(t) \quad (19)$$

The horizontal dependency is described by the Cresman-type horizontal weighting functions with a defined horizontal radius of influence, R_{xy} , which can be written as:

$$W(d) = \frac{R_{xy}^2 - d^2}{R_{xy}^2 + d^2} \quad d^2 \leq R_{xy}^2 \quad (20)$$

$$W(d) = 0 \quad d^2 \geq R_{xy}^2 \quad (21)$$

$$(22)$$

where

$$d^2 = (x - x_0)^2 + (y - y_0)^2 \quad (23)$$

The vertical weighting function is specified after Seaman and is written as:

$$W(z) = 1 - \frac{|z - z_0|}{R_z} \quad |z - z_0| \leq R_z \quad (24)$$

$$W(z) = 0 \quad |z - z_0| > R_z \quad (25)$$

$$(26)$$

where R_z is the vertical radius of influence and z_0 the vertical coordinate of the observation point. If a centered time of influence is chosen, the temporal dependency of the weighting functions can be written as:

$$W(t) = 1 \quad |t - t_0| < \frac{\tau}{2} \quad (27)$$

$$W(t) = \frac{\tau - |t - t_0|}{\tau/2} \quad \frac{\tau}{2} \leq |t - t_0| \leq \tau \quad (28)$$

$$W(t) = 0 \quad |t - t_0| > \tau \quad (29)$$

$$(30)$$

where τ is the half period of the predefined time of influence.

The finite element solution approximates the exact solution ψ by $\hat{\psi}$ using linear basis functions $W(X)$ defined over a domain Ω discretized by E tetrahedral elements and N nodes which can be written as:

$$\psi \approx \hat{\psi} = \sum_{j=1}^N \hat{\psi}_j(t) \omega_j(x) \quad (31)$$

If this approximation is substituted into equation (18) by applying the Galerkin method and by introducing boundary conditions, yields the following system of ordinary differential equations:

$$H(\hat{\Psi})\hat{\Psi} + P(\hat{\Psi})\frac{d\hat{\Psi}}{dt} + q^*(\hat{\Psi}) + r^*(\hat{\Psi}) = 0 \quad (32)$$

where:

$$h_{ij} = \sum_{e=1}^E E \int_{V^e} K_r^e (K_s^e \nabla \omega_j^e \cdot \nabla \omega_i^e) dV \quad (33)$$

$$p_{ij} = \sum_{e=1}^E \int_{V^e} \sigma^e \omega_j^e dV \quad (34)$$

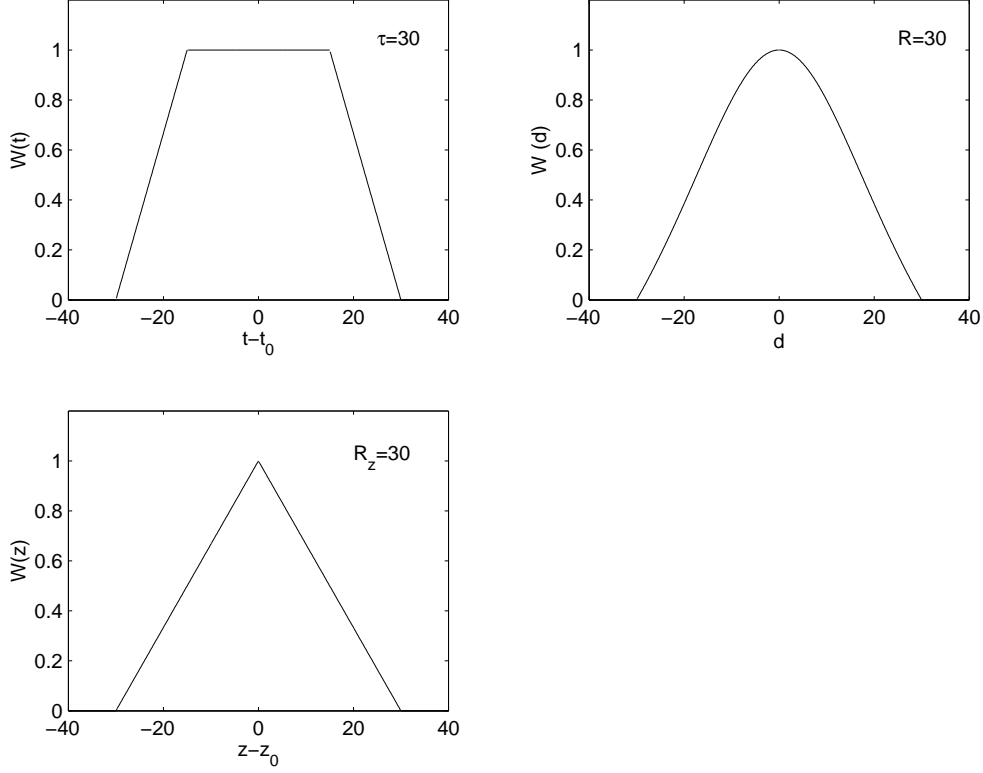


Figure 3: The horizontal, vertical, and temporal dependency of the 4-dimensional weighting functions.

$$q_i^* = \sum_{e=1}^E \left[\int_{V^e} K_r^e K_z z^e \frac{\partial \omega_i^e}{\partial z} dV - \int_{V^e} q^e \omega_i^e dV - \int_{\Gamma_2^e} q_n^e \omega_i^e d\Gamma \right] \quad (35)$$

$$r_i^* = \sum_{e=1}^E \int_{V^e} G^e \frac{\sum_{k=1}^{N_T} \sum_{i=1}^{N_X} W_{ki}^{e2}(X, t) \epsilon_i^e (\theta_{0ki} - \theta_i(t))}{\sum_{k=1}^{N_T} \sum_{i=1}^{N_X} W_{ki}^e(X, t)} \quad (36)$$

where $\theta_{0ki} - \theta_i(t)$ is evaluated at the observation points and is assumed to be constant over the whole element. Equation (32) is integrated in time using a ν -weighted finite difference scheme resulting in:

$$\left(\nu H^{k+\nu} + \frac{P^{k+\nu}}{\Delta t_k} \hat{\Psi}^{k+1} \right) = \left(\frac{P^{k+\nu}}{\Delta t_k} - (1 - \nu) H^{k+\nu} \right) \hat{\Psi}^k - q^{*k+\nu} - r^{*k+\nu} \quad (37)$$

where k and $k + 1$ define the previous and current time levels, Δt_k is the time step size, and H . P , q^* and r^* are evaluated at pressure head

$$\hat{\Psi}^{k+\nu} = \nu \hat{\Psi}^{k+1} + (1 - \nu) \hat{\Psi}^k \quad (38)$$

with $0 \leq \nu \leq 1$. If the Picard iteration is used to linearize equation (37) the final expression is produced, which can be written as:

$$\left(\nu H^{k+\nu,m} + \frac{1}{\Delta t_k} P^{k+\nu,m} \right) \hat{\Psi}^{k+1,m+1} = \quad (39)$$

$$\left(\frac{1}{\Delta t_k} P^{k+\nu,m} - (1 - \nu) H^{k+\nu,m} \right) \hat{\Psi}^k - q^{*k+\nu,m} - r^{*k+\nu,m} \quad (40)$$

where m is the iteration level. This equation can now be solved by standard preconditioned conjugate gradient methods for sparse linear systems.

5 Application of the CATHY model

5.1 Introduction

After the nudging technique had been inserted, the CATHY model has been applied to a testcase. This is a 6 by 11 grid area of 50 by 50 m cells containing a lake in the middle (see Figure 2). Table 1 shows some of the parameter values used for the test case. The location of the five observation points, which are all located at the surface, are indicated as black dots in the figures of the spatially distributed results. For these runs we used mass lumping and Crank-Nicolson time discretization. For the iterations a Picard scheme has been used, and for the soil hydraulic properties the Huyakorn relationship was used with parameter values $\alpha = 0.02$, $\beta = 2$, $\gamma = 2$, $\psi = 0$, residual saturation = 0.333 and $n = 1$. The 10 meter soil profile was discretized into 10 layers, with thicknesses, from top layer to bottom layer, of 1 %, 1 %, 1 %, 5 %, 5 %, 10 %, 10 %, 22 %, 22 %, 23 %. Four different model runs are made:

- initial condition-run
- base-run
- no nudging-run
- nudging-run

The initial condition run is made to achieve initial conditions for the other three runs. The base run represents the “observation data”, which are required for the nudging technique. To separate the base-run from the nudging and no nudging run two different perturbations are made:

- atmospheric perturbation
- initial condition perturbation

In the case of atmospheric perturbation the difference between the base run and the (no)nudging run are the atmospheric conditions, while the initial conditions are the same. In the case of initial condition perturbation the atmospheric conditions are the same but the initial conditions differ.

Table 1: Model parameter values for the test case.

| | |
|-----------------------|---------------|
| K_s | 10^{-4} m/s |
| S_s | 10^{-7} |
| θ_s | 0.35 |
| number of 3D nodes | 924 |
| number of 3D elements | 3960 |
| number of soil layers | 10 |
| soil depth | 10 m |

For testing the nudging technique with these two perturbation runs, the nudging parameters are set to the following base case values: $G = 0.1$, $\epsilon = 1$, $\tau = 1800$ s, $R = 100$ m and $R_z = 2$ m. The effect of varying these base case parameters on the hydrological and numerical results will be described in the next chapter. The results of the application of the CATHY model with the atmospheric perturbation will be discussed in section 5.2 and the results of the application with initial conditions perturbation in section 5.3.

5.2 The atmospheric perturbation run

5.2.1 The influence of the nudging technique on the timestep size

After the implementation of the nudging technique it is also important to analyse the effect of the nudging technique on the computational performance of the model. If after its implementation the model run requires much more time, its applicability should be questioned. An indication for the time required for the model run is the number of timesteps, which are required for the simulation. The model needs about the same time to produce results for small timesteps as for large timesteps. Therefore the number of timesteps can be directly linked to the computation time. The number and size of the timesteps have been analysed for the nudging run as well as for the no-nudging run. The results are shown in Figure 4.

From Figure 4 can be seen that the nudging run is more efficient than the no-nudging run by requiring 24 percent less timesteps for the 4-hour simulation run. This also results in a larger mean timestep for the nudging run compared to the no-nudging run. The maximum time step is limited by a value set by the user and is in the case of the atmospheric perturbation equal to 30 seconds. From this figure it can further be seen that during the assimilation times the timestep size for the nudging run decreases significantly because during these time periods the model results have to be “nudged” towards the observation data, which requires the use of smaller time steps. However the no-nudging run performs really well from about 7000 seconds till the end of the simulation run, using the maximum allowed timestep for the calculation while the nudging run requires much smaller timesteps in this time period. This seems to be in contrast with the larger number of time steps which the no-nudging run uses for the whole simulation period.

To further explore this a histogram has been plotted of the different time step sizes in Figure 5 for the nudging run (left) and the no nudging run (right). From this figure it can be seen that the portion of the smallest timesteps (< 0.8) is much larger in the no-nudging run than in the nudging run. In the histogram of the no-nudging run are there besides the smallest timestep

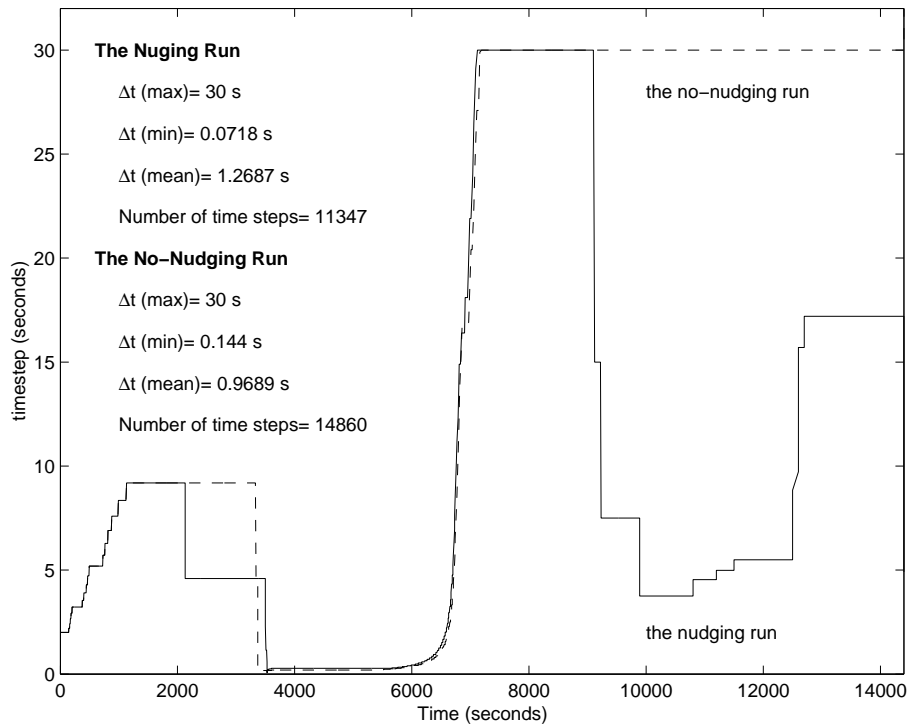


Figure 4: The temporal variation of the timestep size of the nudging and no nudging run for the atmospheric perturbation run.

class only two other classes with a reasonable count (the one of 29.2 - 30.0 sec and the one from 8.4 - 9.2 sec). In the histogram of the nudging run also the largest portion consists of the smallest timestep class but there are also considerable occurrences of timesteps between 0 and 10 seconds, which causes the total number of required time steps to be smaller. Therefore the nudging run is more efficient, despite the fact that the number of maximum allowed timesteps used is significantly smaller compared to the no nudging run.

5.2.2 The influence of the nudging technique on the hydrological results

The primary aim of the implementation of the nudging technique was to improve the hydrological results. To show whether the nudging technique has any influence on the results the computed water table depths for the base run (observed data), the nudging run and the no nudging run are shown in figure 6.

The upper four plots of figure 6 show the water table depths for the base run at different times; The initial time (0 seconds), the first observation time (3600 seconds), which is used for the nudging technique and the second observation time (10800 seconds). The fourth plot at 14400 seconds shows the situation at the end of the simulation.

At time 0 the lake in the middle of the catchment can clearly be distinguished with watertables at the surface. At this time the minimum water table is not below 5 meters below surface. After one hour the water tables depths are totally different. The water level decreases dramatically to -10 meters below surface and only at the depression in the middle the water table remains at the surface. This situation is maintained till the end of the simulation time for

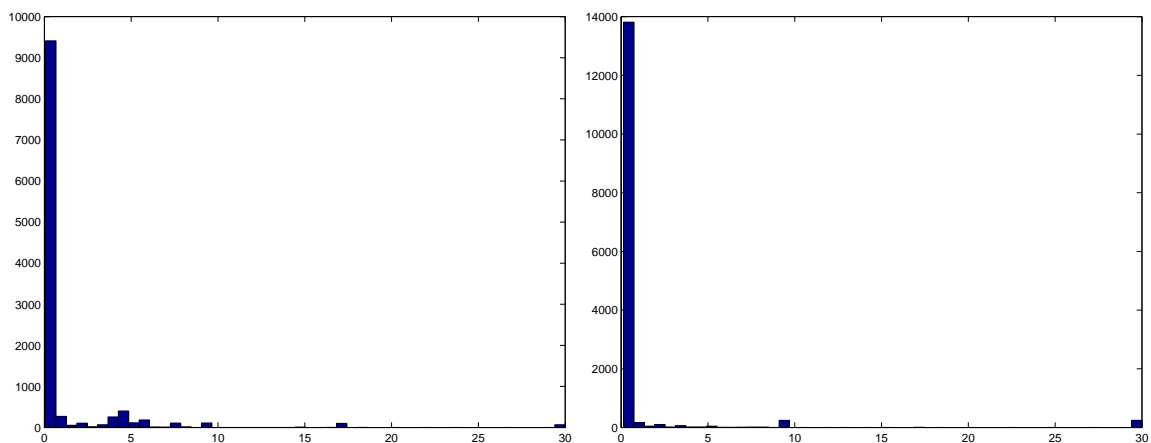


Figure 5: The histogram of timestep size for the nudging (left) and no nudging (right) run for the atmospheric perturbation run

the base run.

In the atmospheric-perturbation run the no nudging run (bottom four graphs of figure 6) has the same initial conditions and therefore shows for time 0 the same water table depths as the base run. At time 3600 seconds the water tables in the depression are still at surface, however at the borders of the depression the water table has decreased compared to the base run due to the high evaporation rates used for the atmospheric perturbation. At time 10800 all water has disappeared from the surface and the water table remains only at 10 meters below surface and lower. This is also the case after four hours.

The nudging run (central four plots) shows the same results for time 0. However at time 3600, the nudge run shows significantly different results compared to the no nudge run. At the borders of the lake the water table is computed much higher which is in a better agreement to the observed values (the base run). Also around the three nudging points located south-east of the depression a correction, in this case an increase of the height of the watertable, towards the base run can be noticed. For the last two timesteps a correction has been made around the two nudging points which are located north-east of the depression. Figure 6 shows that the implementation of the nudging technique leads to a better agreement with the observed values.

Figure 6 shows the effect of the nudging technique on the spatial distribution of the water tables. To investigate the influence of the nudging technique on the spatial distributed computed error in surface soil moisture values, the difference in these surface soil moisture values between the observed data (base run) and the computed data have been plotted for both the nudging and the no nudging run in Figure 7.

This figure shows the difference in water saturation at the surface nodes between the base run and the no nudging run (top four graphs) and the difference between the base run and the nudging run (bottom four graphs) at four different times for the atmospheric perturbation run. Because the initial conditions are the same for all three runs the difference at time 0 between the base run and the (no) nudging run is by definition 0. For the no nudging run at time 3600 seconds an increase in the difference between the base run and the no nudging run can be noticed, especially outside the depression to reach an mean areal difference of 0.2997. At time 10800 seconds the largest differences can be seen in the boundaries of the depression

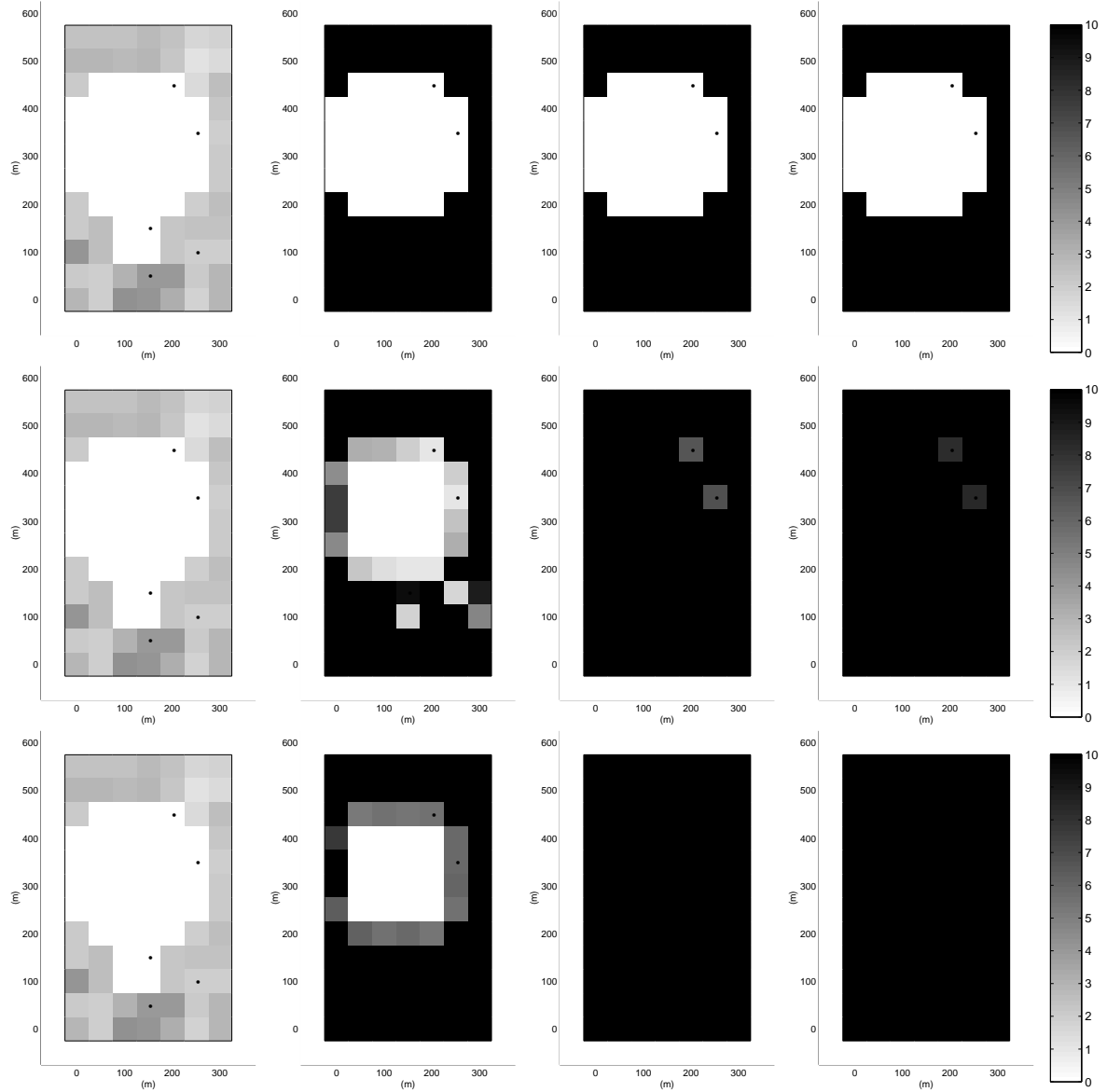


Figure 6: The water table depths for the base run (top four plots), the nudging run (central four plots) and the no nudging run (bottom four plots) for the atmospheric perturbation run at four different times: $t = 0$, $t = 3600$, $t = 10800$ and $t = 14400$ seconds (from left to right).

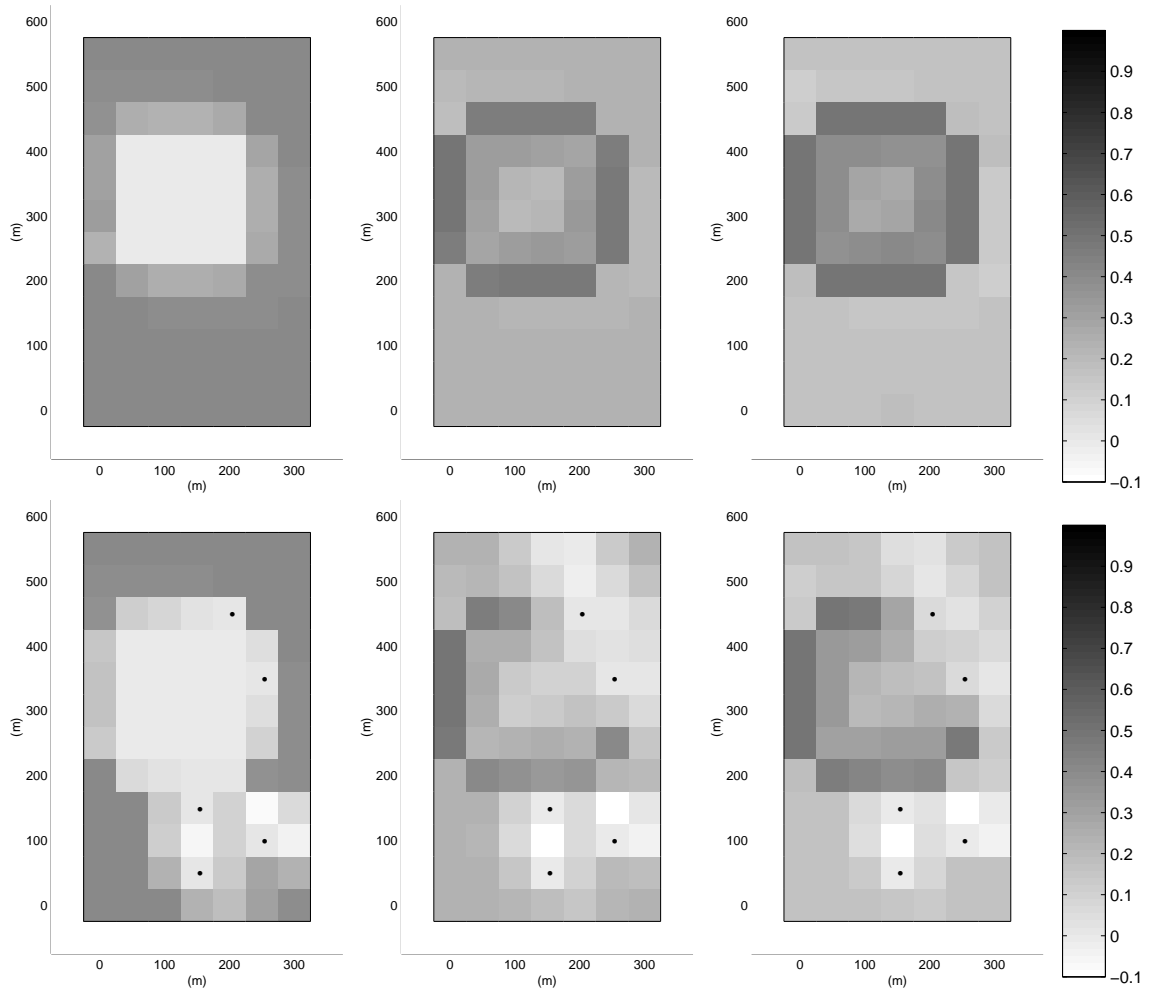


Figure 7: The difference in water saturation at the surface nodes between the base run and the no nudging run (top three graphs) and between the base run and the nudging run (bottom three graphs) at three different times (3600, 10800 and 14400 seconds) for the atmospheric conditions perturbation run

and at this time the mean spatial difference is 0.2861. At time 14400 this mean difference has decreased to 0.2646. From these four graphs can also be seen that the results of the no nudging run are always less than or equal to the base run (with the exception of the lake cells at $t = 3600$).

Figure 7 shows for the nudging run a different spatial distribution of the difference in soil moisture at the surface nodes. At time 0 the difference is 0 as a result of the same initial conditions. At time 3600 seconds an increase in the difference can be noticed. However at and around the nudging points, especially the three located south-east of the lake, this increase is much smaller. For some grid cells the nudge run even overshoots the results of the base run, which explains that the difference between the two is sometimes negative. The mean difference between the base run and the nudging run at the first observation time is 0.2036, which is a decrease of 32 percent compared to the no-nudging run at the same time. After 10800 seconds a bigger influence of the two nudging points located north of the lake can be noticed, resulting in a further decrease of the mean difference to a value of 0.1785. Compared to the difference at the same time between the base run and the no-nudging run this is an improvement of almost 38 percent. At time 14400 the influence of the five nudging points can still be seen, however the mean difference has again increased, due to this time is located outside the assimilation period, to a value of 0.1888, which is still an improvement of 29 percent compared to the no nudging run.

From Figure 7 it can clearly be concluded that the implementation of the nudging technique leads to an improvement in the mean error of soil moisture values at the surface nodes using the atmospheric perturbation run. This improvement is not only made during the assimilation times but also outside the periods of nudging influence.

After having seen the effect of the nudging technique on the spatial behavior of the water table depths and the surface soil moisture values, its influence on the temporal distribution of soil moisture values has also been investigated at the five nudging points and the results have been plotted in Figure 8.

Figure 8 shows the results of the four-hour evaporation test case showing the temporal variation of the soil moisture content at the five nudging points. The base run represents the “soil moisture observation data” at these nodes during the assimilation times. These assimilation times are indicated between the black lines with $\tau/2$ of half an hour before and after T_{obs}^1 and T_{obs}^2 . In this case of atmospheric perturbation the evaporation input, which has been used for the base run is perturbed and a nudging run and a no nudging-run is made. The increase in evaporation between 2 and 3 hours can be explained by discharge flowing out of the “lake” into cells located downstream of the lake. From Figure 8 it can clearly be seen that until the start of the assimilation time the nudging run is exactly the same as the no nudging run. After time equals 1800 seconds the nudging technique is activated and differences between the nudging and no nudging technique can be seen. In the upper two graphs the effect of this technique can only be seen at about 1 hour because before the nudging and no nudging runs both equal the observation data. Clearly it can be seen that the soil moisture values of the nudging run are driven towards those of the base run during the assimilation time to reach a better agreement between these two. After the assimilation period, when the nudging technique is inactive again, generally an immediate increase in the difference between the nudging run and the observation data can be seen.

A small time lag of the increase in soil moisture values between the two “assimilation periods” can be noticed as well as a difference in amount of increase between the nudging and the no

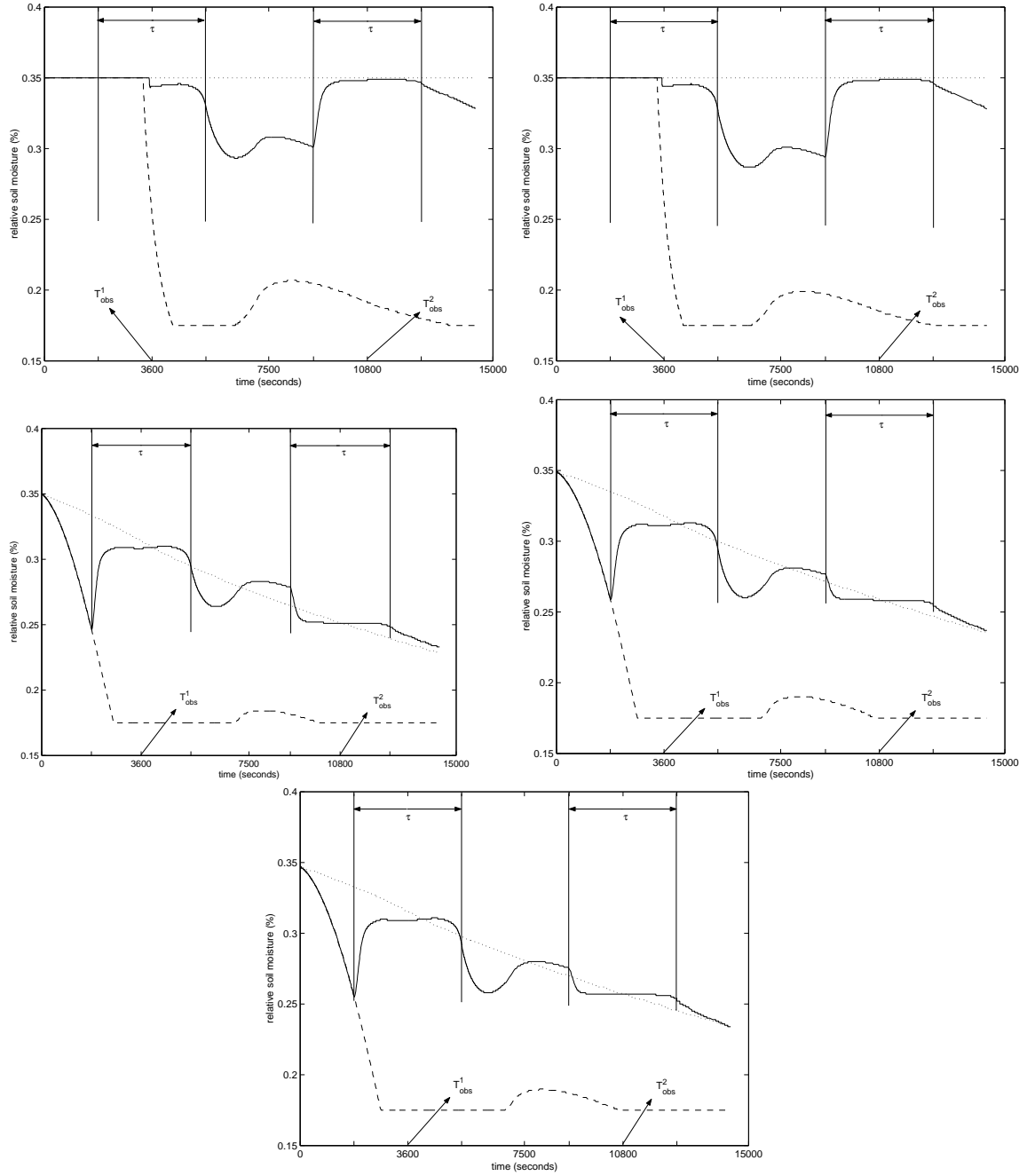


Figure 8: The temporal variation of soil moisture at the five observation points for the base run (dotted line), no nudge run (dashed line) and the nudge run (solid line) performed by the atmospheric perturbation run with the two observation times at 3600 s and 10800 s. The nudging parameter values used are: $G=0.1$, $\epsilon = 1$, $\tau = 1800s$, $R_{xy} = 100$ m, and $R_z = 2$ m. Note that τ in the figures should have been 2τ

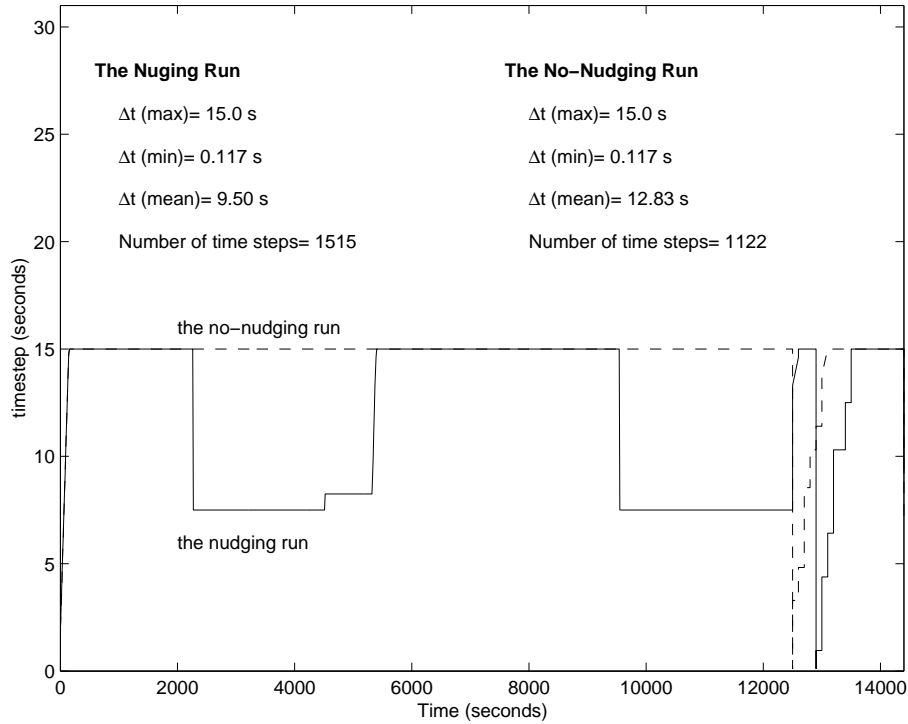


Figure 9: The temporal variation of the timestep size for the initial conditions perturbation run.

nudging run. In the upper two graphs the increase in soil moisture is largest for the no nudging run while for the bottom three graphs the increase is larger in the nudging run. These differences however take place outside the time period in which the nudging technique is active and are caused by different soil moisture contents and not by the nudging technique.

5.3 The initial conditions perturbation run

5.3.1 The influence of the nudging technique on the timestep size

Besides the atmospheric perturbation run also a run with different initial conditions for the base run compared to the nudging and no nudging run has been made. For the initial conditions perturbation run a totally different behavior of the temporal variation of the timestep size can be seen compared to the atmospheric perturbation run. First of all the value of the maximum allowed timestep is 15 seconds and further this run required much fewer time steps than the atmospheric perturbation run. A reason for this is probably the “unforced” input values of evaporation.

The no-nudging run contains the maximum timestep size for almost the whole simulation period with an exception at the end, while the timestep size for the nudging run decreases significantly during the assimilation times. The decrease in time step during the assimilation times is the reason why the nudging run uses more timesteps than the no-nudging run. Around time 12500 sec the value of Δt suddenly decreases dramatically for the no-nudging run followed in delay by the nudging run, which shows exactly the same behavior in decrease. These decreases in time step size are caused by numerical instability at these times. A reason

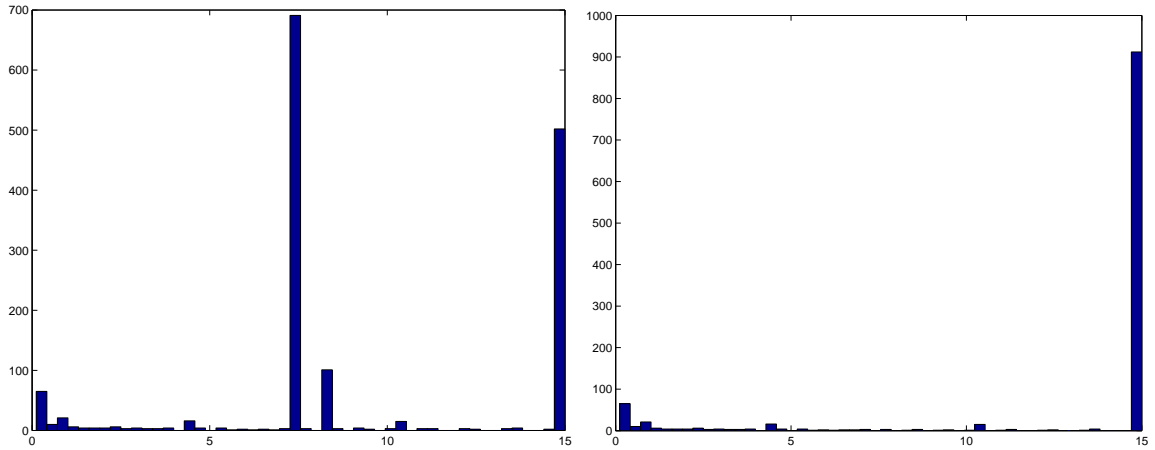


Figure 10: The histogram of timestep size for the nudging (left) and no nudging (right) run for the initial conditions perturbation run

for this numerical instability has not be found.

Figure 10 shows the histograms of the timestep size for the nudging run (left) and the no nudging run (right) for the initial conditions perturbation run. From Figure 10 it can be seen that for the no nudging run almost all timesteps are the maximum allowed 15 seconds with the exception of a few very small time steps caused by the numerical instability at time 12500 seconds. The histogram of the nudging run also contains a lot of the maximum allowed timestep, however the most occurred timestep size is around 7 seconds. Also a timestep size of eight seconds occurs quite often. This is due to the effect of the nudging technique which decreases the used time step to about 7.5 during the assimilation time (see Figure 9). Further there is also for the nudging run a considerable amount of the small timestep sizes caused by the numerical instability at around 12800 seconds.

Compared to the atmospheric perturbation run, the smaller time steps play a less important role in the initial condition perturbation run. Therefore also the required number of timesteps is much smaller for the initial condition run than for the atmospheric perturbation.

5.3.2 The influence of the nudging technique on the hydrological results

For the initial perturbation run the effect of the nudging has been analysed for the same hydrological variables as was done for the atmospheric perturbation run. Figure 11 shows the influence of the nudging technique on the spatial distribution of the water table depths at four different times (from left to right; $t = 0$ s, $t = 3600$ s, $t = 10800$ s and $t = 14400$ s). The top four plots are the values as computed with the base run, the central four as computed with the nudging run and the bottom four as computed with the no nudging run. The base run shows a completely different distribution at time is 0 as a result of different initial conditions. The effect of the nudging technique can only be seen at $t = 14400$ s, which shows for the nudging run at the borders of the topographic depression higher computed water tables compared to the no nudging run, which is in better agreement with the observed values as generated by the base run.

The spatial distributed error between the computed and observed values has been plotted

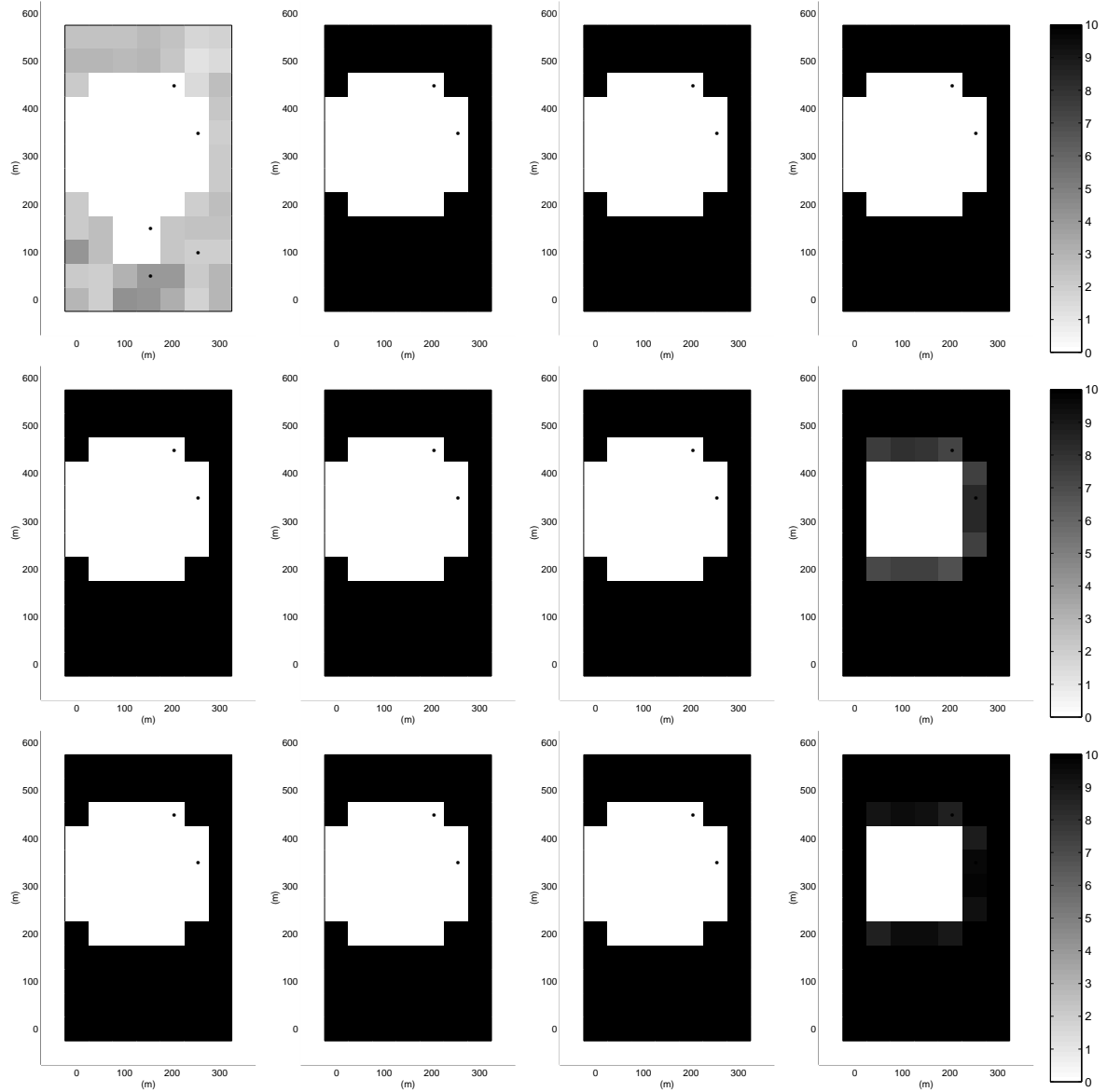


Figure 11: The water table depths for the base run (top four plots), the nudging run (central four plots) and the no nudging run (bottom four) for the initial conditions perturbation run at 4 different times: $t = 0$, $t = 3600$, $t = 10800$ and $t = 14400$ seconds (from left to right).

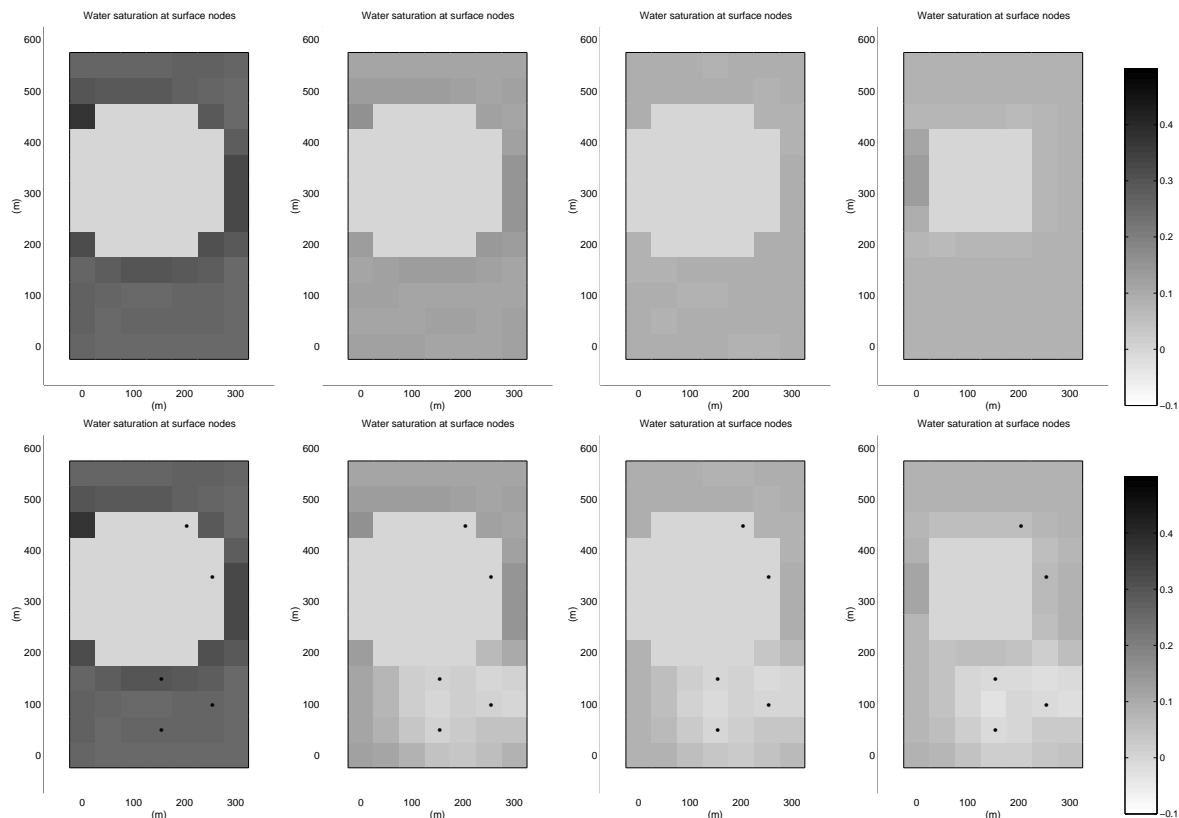


Figure 12: The difference in water saturation at the surface nodes between the base run and the no nudging run (top four graphs) and between the base run and the nudging run (bottom four plots) for the initial conditions perturbation run at four different times: $t = 0$, $t = 3600$, $t = 10800$ and $t = 14400$ seconds (from left to right).

for the no nudging run (top four plots) and the nudging run (bottom four plots) in Figure 12. This figure shows a same behavior as Figure 7 with decreasing computed errors for the nudging run at and around the five nudging points. The initial mean areal difference is for both runs 0.1695. At the first observation time this error has decreased for the nudging run till 0.0509, while the error of the no nudging run only decreases till 0.0748. At the second observation time the error for the nudging run has further decreased to 0.0365 and for the no nudging run this error reaches a value of 0.0551. At the end of the simulation these errors have again increased because the nudging technique is not active anymore to become respectively 0.0448 and 0.0660. From these values and the plots can be concluded that also for the initial perturbation run the computed surface soil moisture values improve when using the nudging technique.

To see the effect of the nudging technique on the temporal variation of the soil moisture at the nudging nodes, also for the initial conditions perturbation run this temporal variation of the soil moisture at these five nudging points has been investigated. Figure 13 shows the temporal variation of the soil moisture at the five nudging points for the base run, the no nudging run and the nudging run as calculated by the initial condition perturbation run. The top two plots show a saturated soil for all of the runs for almost the whole simulation period. Only a small decrease in soil moisture can be noticed after around 12000 seconds. But even here a difference between the nudging and the no nudging run can be seen. During the end of the assimilation time when the no nudging run already decreases, the nudge run stays saturated

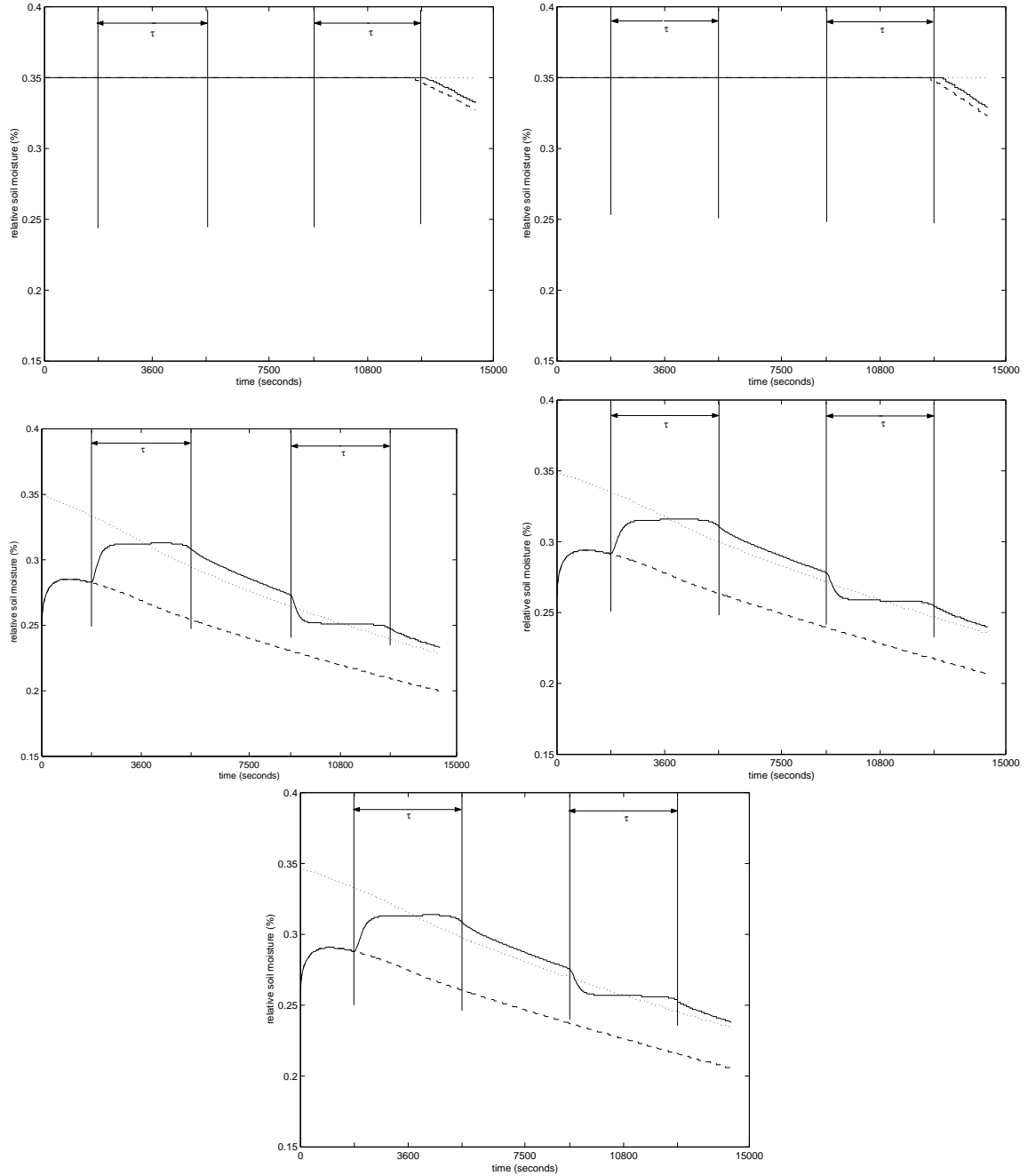


Figure 13: The temporal variation of soil moisture at the five observation points for the base run (dotted line), no nudge run (dashed line) and the nudge run (solid line) performed by the initial condition perturbation run with the two observation times at 3600 s and 10800 s. The nudging parameter values used are: $G=0.1$, $\epsilon = 1$, $\tau = 1800s$, $R_{xy} = 100$ m, and $R_z = 2$ m

for these two nodes. Even after the assimilation time has ended it takes a while before the nudging run starts to decrease.

The other three nodes show a more interesting behavior. At time 0 the base run differs significantly from the nudging and no nudging run as a result of different initial conditions. Until the beginning of the first assimilation time the nudge run and the no nudge run are (by definition) exactly the same. However at the beginning of the assimilation time it can be seen that the nudging run is immediately corrected upward, towards the base run, while the no nudging run remains decreasing. Also after the first assimilation time the results of the nudging run remain close to those of the base run as a result of the same atmospheric inputs. Therefore the correction which has to be made at the second observation point is much smaller compared to the first assimilation point or the corrections at the atmospheric perturbation run. Also after the second assimilation time has ended the nudging run remains till the end of the simulation very close to the observation data. Therefore it can be concluded from Figure 13 that also for the initial condition perturbation runs, the implementation of the nudging technique considerably decreases the error between the computed values and the observed values.

6 The influence of the nudging parameters

6.1 Introduction

After having seen the influence of the nudging technique on the hydrological results in the previous chapter, this chapter describes the influence of some nudging parameters on the nudging effect. The influence of different values for the nudging parameters has been investigated in terms of hydrological as well as computational behavior, using the atmospheric perturbation scenario. Section 6.2 describes the influence of G , section 6.3 the influence of R_{xy} and section 6.4 the influence of τ on the hydrological and computational results.

6.2 The influence of G

Table 2 shows the effect of different G values on some numerical and computational results. From this table it can be concluded that for small values of G (till $G = 0.1$) the cumulative absolute mass balance error is generally smaller compared to the no nudge run while larger G -values show a small increase in the cumulative absolute mass balance error. However the cumulative relative mass balance error is smallest for the no nudging run. The total number of required back-stepping occurrences is for G -values till 0.3 relatively small. For G -values of 0.5 and higher this number increases rapidly due to numerical instability. The total CPU reaches a minimum for $G=0.005$ of 837 seconds, which is almost 44 percent less than required for the no nudging run. However for G -values of 0.5 and higher this total CPU increases rapidly. The number of total timesteps shows a similar behavior and also reaches a minimum for $G = 0.005$ of 6827 timesteps, which is a decrease of 29 percent compared to the no nudging run.

The minimum timestep size is large for the no nudging run and for the run with $G = 10^{-3}$. For G -values higher than 10^{-3} the minimum timestep size decreases and even reaches the minimal allowed timestep size twice (for $G = 0.005$ and $G = 0.1$). For G -values of 0.3 and higher there are a lot of back-stepping occurrences but the minimal allowed timestep size is never reached for

Table 2: The effect of the different G-values on the numerical and computational results. Note that “Total timesteps” does not include back-stepping occurrences.

| | | | | |
|----------------------------|----------------------|----------------------|----------------------|----------------------|
| G-values | no-nudge | 0.001 | 0.005 | 0.01 |
| Cum. abs. mass bal. error | $1.64784 \cdot 10^4$ | $1.58407 \cdot 10^4$ | $1.37183 \cdot 10^4$ | $1.35106 \cdot 10^4$ |
| Cum. rel. mass bal. error | -5.70785 | -6.18765 | -7.05843 | -7.41774 |
| Total back-stepping occur. | 1 | 1 | 12 | 2 |
| Total CPU for the simul. | 1408 | 1315 | 837 | 1393 |
| Total timesteps | 9655 | 11173 | 6827 | 10593 |
| Smallest timestep | 0.125 | 0.25 | 0.0001221 | 0.03125 |
| Largest timestep | 32 | 32 | 32 | 32 |
| Average timestep | 1.491 | 1.289 | 2.109 | 1.359 |
| Avg NL iter. per timestep | 4.20 | 4.02 | 4.30 | 4.04 |
| G-values | 0.05 | 0.1 | 0.3 | 0.5 |
| Cum. abs. mass bal. error | $1.64016 \cdot 10^4$ | $1.57571 \cdot 10^4$ | $1.66649 \cdot 10^4$ | $1.62116 \cdot 10^4$ |
| Cum. rel. mass bal. error | -9.43828 | -9.10268 | -9.61364 | -9.36321 |
| Total back-stepping occur. | 4 | 10 | 5 | 452 |
| Total CPU for the simul. | 1165 | 1040 | 1612 | 1901 |
| Total timesteps | 6959 | 7196 | 12535 | 9656 |
| Smallest timestep | 0.007813 | 0.0001221 | 0.0004883 | 0.0004883 |
| Largest timestep | 32 | 32 | 32 | 32 |
| Average timestep | 2.069 | 2.001 | 1.149 | 1.491 |
| Avg NL iter. per timestep | 4.25 | 4.34 | 4.27 | 6.64 |
| G-values | 0.8 | 1.0 | 10.0 | |
| Cum. abs. mass bal. error | $1.65944 \cdot 10^4$ | $1.65472 \cdot 10^4$ | $1.71729 \cdot 10^4$ | |
| Cum. rel. mass bal. error | -9.58681 | -9.53248 | -9.83784 | |
| Total back-stepping occur. | 1631 | 2121 | 31299 | |
| Total CPU for the simul. | 5564 | 5137 | 81385 | |
| Total timesteps | 14624 | 16104 | 54157 | |
| Smallest timestep | 0.0004883 | 0.0004883 | 0.0002441 | |
| Largest timestep | 32 | 32 | 32 | |
| Average timestep | 0.9847 | 0.8942 | 0.2659 | |
| Avg NL iter. per timestep | 9.82 | 10.70 | 32.12 | |

Table 3: The influence of G on the mean spatial difference of the soil moisture at the surface nodes between the base run and the nudging run at three different times for the atmospheric perturbation run.

| time (seconds) | 3600 | 10800 | 14400 |
|----------------|--------|--------|--------|
| no nudging run | 0.2997 | 0.2861 | 0.2646 |
| $G = 10^{-4}$ | 0.2992 | 0.2832 | 0.2638 |
| $G = 10^{-3}$ | 0.2934 | 0.2484 | 0.2521 |
| $G = 0.005$ | 0.2622 | 0.1867 | 0.2036 |
| $G = 0.01$ | 0.2364 | 0.1777 | 0.1928 |
| $G = 0.05$ | 0.2063 | 0.1775 | 0.1888 |
| $G = 0.1$ | 0.2036 | 0.1785 | 0.1888 |
| $G = 0.3$ | 0.2020 | 0.1795 | 0.1887 |
| $G = 0.5$ | 0.2018 | 0.1802 | 0.1887 |
| $G = 0.8$ | 0.2016 | 0.1804 | 0.1886 |
| $G = 1.0$ | 0.2017 | 0.1805 | 0.1885 |
| $G = 10.0$ | 0.2015 | 0.1813 | 0.1883 |

these runs. For all runs the largest time step reaches the maximal allowed timestep which is in this case 32 seconds. The average time step is largest for the run with $G = 0.005$ but also the runs with G -values of 0.05 and 0.1 have an average timestep size which is larger than 2 seconds. For the nudging runs with G -values of 0.8 and 1.0 the average timestep becomes smaller than 1 second. The average nonlinear iterations per timestep generally remains between 4.0 and 4.3 for G -values till 0.3 while for higher G -values this number increases to reach a value of 32.12 when $G = 10$.

Table 3 shows the effect of the G term on the mean spatial error of the soil moisture at the surface nodes for the nudging runs compared to the base run at three different times. For the no nudging run the mean difference is largest at time 3600 and smallest for time 14400. For the nudging runs however the smallest mean difference can be seen at the second observation time due to the nudging technique and shows an increase in the error for t is 14400.

For a G -value of 10^{-4} the mean difference is close to those values of the no nudging run. However for increasing G -values an decreasing mean difference can be seen. For the first observation time this decrease goes on till $G = 0.8$ after which it slightly increases for $G = 1$. However after $G = 0.05$ the increase of the improvement decreases. For the run with $G = 0.05$ the improvement compared to the no nudge run is 31.2 percent while for $G = 0.8$ this improvement is 32.7 percent. The same behavior can be seen at time 14400 s, at which however the improvement stabilizes after $G = 0.05$.

The results for the second observation time show a slightly different behavior in the decrease of the difference. For this time it reaches a minimum for the run with $G = 0.05$ and shows increasing values for higher G -values. Therefore and, taking into account the higher required CPU for the larger G -values (see table 2), in this case for the spatial distribution of soil moisture content at the surface nodes the optimal G -value is around 0.05.

From Table 4 can be seen that the variance of the difference between the observed and the computed values of surface soil moisture decrease with increasing values of G to reach a

Table 4: The influence of G on the variance (σ) of the differences between the base- and nudging run of the spatial soil moisture values at the surface nodes averaged over the whole simulation time.

| G-value | σ | G-value | σ |
|------------|----------|----------|----------|
| G = 0.0001 | 0.0281 | G = 0.3 | 0.0233 |
| G = 0.001 | 0.0260 | G = 0.5 | 0.0233 |
| G = 0.005 | 0.0233 | G = 0.8 | 0.0233 |
| G = 0.01 | 0.0226 | G = 1.0 | 0.0233 |
| G = 0.05 | 0.0231 | G = 10.0 | 0.0233 |
| G = 0.1 | 0.0232 | | |

minimum value of 0.0226 at $G = 0.01$. For a G value of 0.1 σ has increased to 0.232 and for G -values 0.3 till 1.0 the variance remains the same.

Figure 14 shows the effect of the value of G on the temporal variation of soil moisture values at the five nudging points. Figure 14 shows the results of seven nudging runs, all with different values of G together with the base run and the no nudging run. The thick line represents the observation data and the dotted line the no nudging run. The nudging runs are labeled 1 to 6 representing the G values respectively of 10^{-4} , 10^{-3} , 0.005, 0.01, 0.1 and 0.5. From the bottom three graphs of Figure 14 it can be seen that the higher the value of G, the stronger the computed data are driven towards the observation data. Compared to the run with $G = 0.1$, which has been used in all previous runs, the run with $G = 0.5$ converges better to the base run and for G-values below 0.1 the opposite can be seen. For $G = 10^{-3}$ almost no effect can be seen during the first assimilation time, however during the second assimilation time a clear difference between the nudging and no nudging run can still be seen. For a G-value of 10^{-4} also this difference at the second assimilation time has mostly disappeared. Between the results of the nudging runs with G-values from 0.3 to 1 almost no distinction in the temporal variation of soil moisture values at the nudging points can be seen. Therefore this category is in this figure only represented by $G = 0.5$.

Besides this difference in stronger or less strong convergence to the observation data a second difference between the several nudge runs can be noticed from this figure. The higher the values of G the quicker the response of the nudge run. For the run with the G-value of 0.5 the increase at the first assimilation time and the decrease at the second assimilation time are much "steeper" compared to the runs with lower G-values. From the top two plots a same effect of the different G-values can be concluded; the higher the values of G, the stronger and sooner is the convergence towards the observation data. Also for these nodes it is shown that for a G-value of 10^{-4} the influence of the nudging is nil.

Figure 15 shows the difference in temporal variation of the soil moisture values at two of the five nudging points for G-values of 0.1, 1 and 10. From this figure it can be concluded that despite the very strong effect of $G = 10$ on the numerical results, its effect on the hydrological results is relatively small.

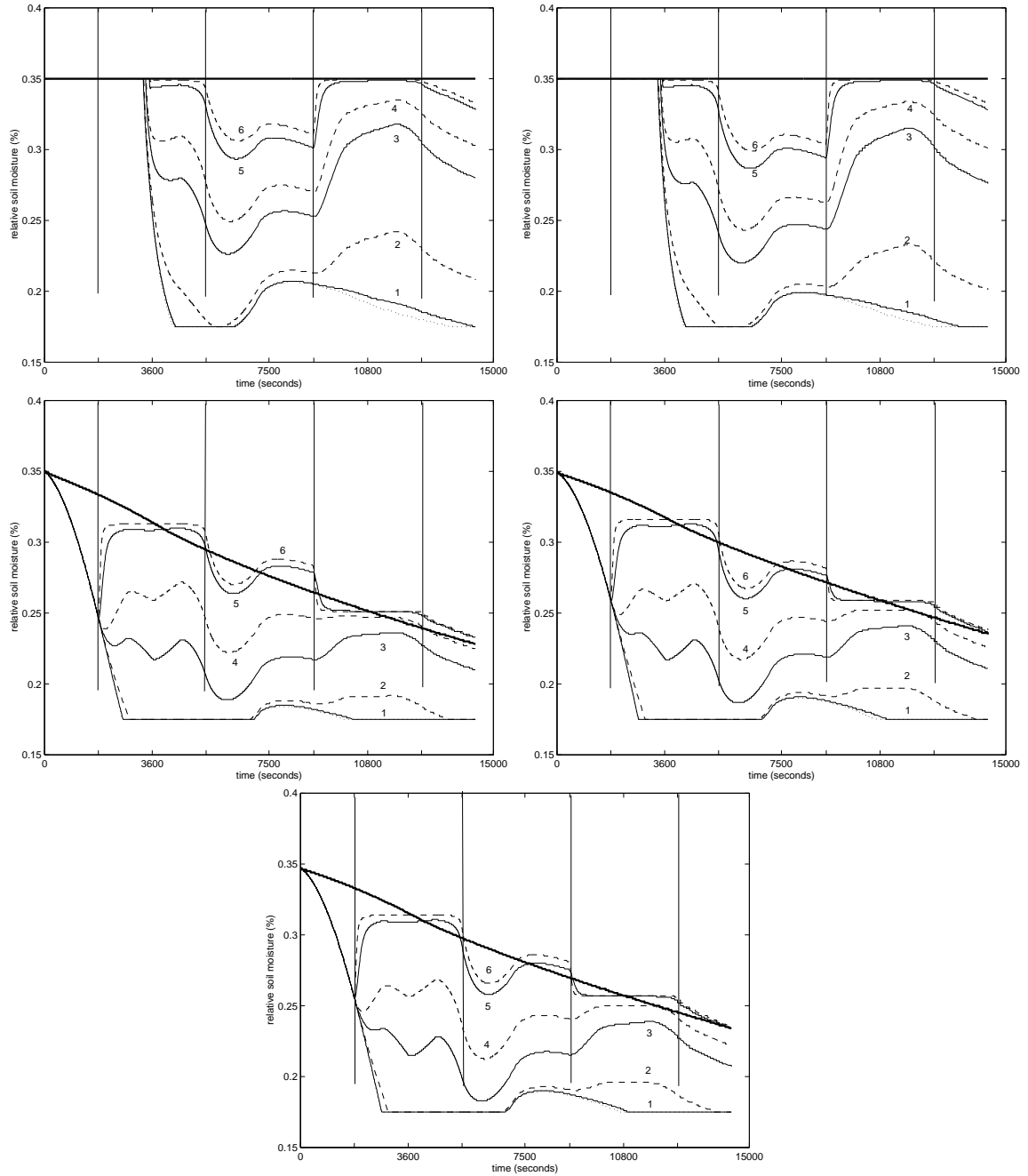


Figure 14: The influence of G on the temporal behavior of the soil moisture content at the five nudging points together with the base run (thick line) and the no nudging run (dotted line). 1: $G = 10^{-4}$, 2: $G = 10^{-3}$, 3: $G = 0.005$ 4: $G = 0.01$, 5: $G = 0.1$, 6: $G = 0.5$

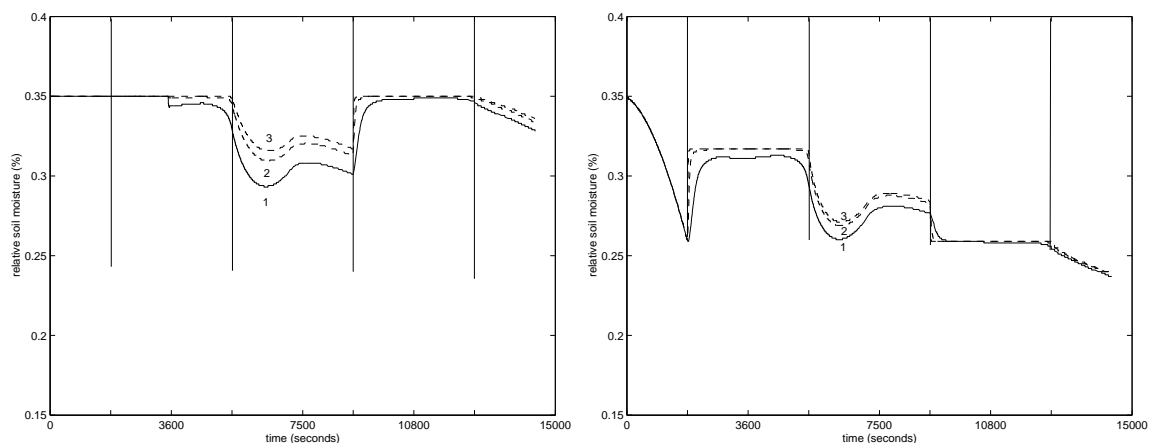


Figure 15: The influence of high G-values on the temporal behavior of the soil moisture content at two nudging points 1: $G = 0.1$, 2: $G = 1$, 3: $G = 10$

6.3 The influence of R_{xy}

After the influence of G on the nudging effect had been investigated, the effect of the horizontal radius of influence of the nudging technique (R_{xy}) on the same variables was investigated.

Table 5 shows the influence of R_{xy} on the numerical and computational results. The cumulative absolute mass balance error generally increases with increasing R_{xy} -value, and stabilizes for R_{xy} values of 150 m and higher. The total back-stepping occurrences are low for the no-nudge run and the run with $R_{xy}=50$. For the runs with higher R_{xy} -values the total back-stepping occurrences are about 11 with the exception for $R_{xy} = 200$, which only has 4 back-stepping occurrences. This run also has a very low CPU of only 622 seconds, which is a decrease of 56 percent compared to the no nudge run. Also the number of required timesteps reaches a minimum of 4565 for this run, which is a decrease of 53 percent compared to the no nudging run. For the total CPU and the number of timesteps the nudging run with $R_{xy} = 50$ performs worst. However for this run the minimum required timestep size is relatively high, while for the runs with $R_{xy} = 100, 150$ and 250 meter the minimum allowed timestep size is reached. For all runs the timestep size reaches the maximum allowed size of 32 seconds. The average timestep over the simulation exceeds 2.0 for all runs with R_{xy} -values of 100 m and larger and reaches a maximum for $R_{xy} = 200$ with an average timestep which is even larger than 3 seconds. The average nonlinear iterations per timestep is for all runs between 4.1 and 4.5.

Figure 16 shows the influence of R_{xy} on the spatial distribution of the nudging effect for the difference in the water saturation at the surface nodes between the base run and the nudging run. The results have been plotted for three different times: 3600 s (left column), 10800 s (central column) and for $t = 14400$ s (right column) for three nudging runs with different R_{xy} -values. The three plots at the top show the results for the nudging run with $R_{xy} = 50$ m, the three plots in the middle those for $R_{xy} = 150$ m and the three plots at the bottom the results for $R_{xy} = 250$ m.

From the results for the run with $R_{xy} = 50$ m can clearly be seen that the nudging effect is restricted to an area close to the nudging points. Only the grid cells in which the nudging points are located show a clear decrease in the difference between the computed and observed data. This behavior changes when R_{xy} increases. From the run with R_{xy} -values equal to

Table 5: The effect of the different R_{xy} -values on the numerical and computational results.

| R-values ($G = 0.1, \tau = 1800$) | no-nudge | 50 | 100 |
|-------------------------------------|----------------------|----------------------|----------------------|
| Cum. abs. mass bal. error | $1.64784 \cdot 10^4$ | $1.65996 \cdot 10^4$ | $1.57571 \cdot 10^4$ |
| Cum. rel. mass bal. error | -5.70785 | -7.06258 | -9.10268 |
| Total back-stepping occur. | 1 | 2 | 10 |
| Total CPU for the simul. | 1408 | 1486 | 1040 |
| Total timesteps | 9655 | 12079 | 7196 |
| Smallest timestep | 0.125 | 0.0312 | 0.0001221 |
| Largest timestep | 32 | 32 | 32 |
| Average timestep | 1.491 | 1.192 | 2.001 |
| Avg NL iter. per timestep | 4.20 | 4.13 | 4.34 |
| R-values ($G = 0.1, \tau = 1800$) | 150 | 200 | 250 |
| Cum. abs. mass bal. error | $1.62903 \cdot 10^4$ | $1.57991 \cdot 10^4$ | $1.47116 \cdot 10^4$ |
| Cum. rel. mass bal. error | -10.8507 | -11.0386 | -10.8640 |
| Total back-stepping occur. | 11 | 4 | 11 |
| Total CPU for the simul. | 910 | 622 | 954 |
| Total timesteps | 7076 | 4565 | 6771 |
| Smallest timestep | 0.0001221 | 0.003906 | 0.0001221 |
| Largest timestep | 32 | 32 | 32 |
| Average timestep | 2.035 | 3.154 | 2.127 |
| Avg NL iter. per timestep | 4.26 | 4.46 | 4.32 |

Table 6: The influence of R_{xy} on the mean spatial difference of the soil moisture at the surface nodes between the base run and the nudging run at three different times for the atmospheric perturbation run.

| time | 3600 | 10800 | 14400 |
|----------------|--------|--------|--------|
| no nudging run | 0.2997 | 0.2861 | 0.2646 |
| R = 50 | 0.2580 | 0.2424 | 0.2361 |
| R = 100 | 0.2036 | 0.1785 | 0.1888 |
| R = 150 | 0.1913 | 0.1614 | 0.1754 |
| R = 200 | 0.1891 | 0.1577 | 0.1731 |
| R = 250 | 0.1718 | 0.1454 | 0.1630 |

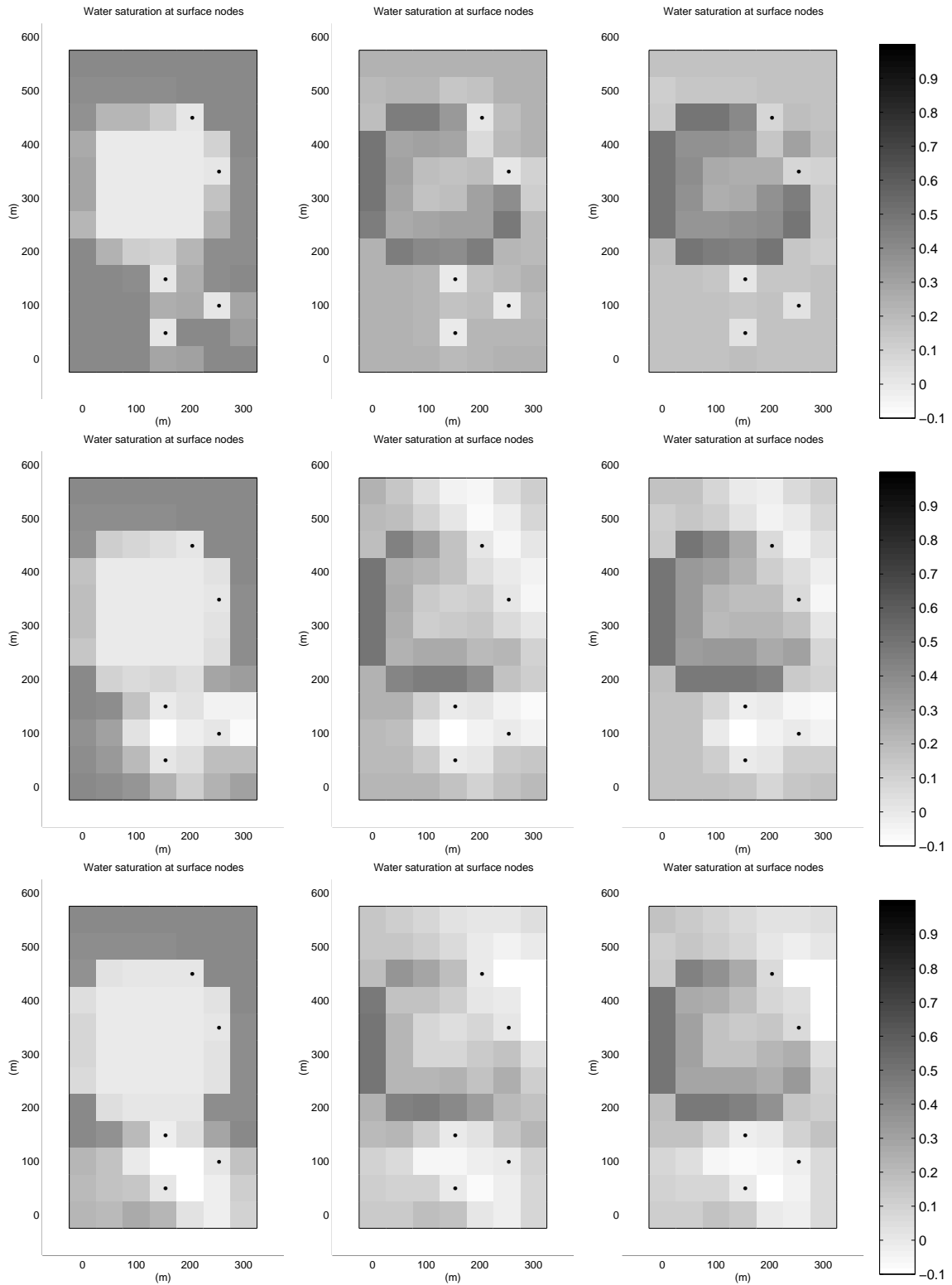


Figure 16: The influence of R_{xy} on the spatial distribution of the difference between the base and nudging run. The upper three graphs show the results at the times (from left to right) 3600, 10800 and 14400 for $R_{xy} = 50$ m, the three plots in the center for $R_{xy} = 150$ m and the bottom three graphs for $R_{xy} = 250$ m.

Table 7: The influence of R_{xy} on the variance (σ) of the differences between the base- and nudging run of the spatial soil moisture values at the surface nodes averaged over the whole simulation time.

| R-value | σ |
|-----------|----------|
| R = 50 m | 0.0258 |
| R = 100 m | 0.0232 |
| R = 150 m | 0.0226 |
| R = 200 m | 0.0219 |
| R = 250 m | 0.0206 |

150 m it can be seen that the area of influence has increased. Not only the grid cells in which the nudging points are located show a better agreement of the nudging run with the base run but also the surrounding cells show a clear improvement. At time 3600 this is only the case for the three bottom nudging points. However at the second observation time and at the end of the simulation this wider spatial influence of the nudging technique can be seen for all the nudging points.

This increase in the spatial influence of the nudging technique leads to a significant improvement of these results. The mean difference between the base- and nudging run clearly decreases with increasing R_{xy} -values (Table 6). From this table it can be seen that for all times the error in the spatially calculated surface soil moisture decreases with increasing R_{xy} -values. But even the results for the run with R_{xy} -value equals to 50 m an average improvement of 13.3 percent in the results compared to the no nudging run can be noticed. For $R_{xy} = 250$ this improvement has increased to 43.4 percent. Further it can be seen from Table 6 that the influence of larger R_{xy} -values is biggest at the two observation times but also at time 14400, which is one hour after the second observation time and half an hour after the nudging technique has ended, a considerable improvement of the results compared to the no nudging run can still be seen.

Figure 16 also shows that for the run with $R_{xy} = 250$ m the decrease in the error compared to the run with $R_{xy} = 150$ m can be seen for most cells. However for some grid cells (for example (300,100), (300,150) and (250,150)) the run with $R_{xy} = 250$ m shows an increased difference between the base and nudging run. However the mean difference of the run with $R_{xy} = 250$ m shows an improvement of more than 9 percent compared to the run with $R_{xy} = 150$ m. From Figure 16 and Table 6 it can therefore be concluded that increasing values of R_{xy} lead to a better spatial agreement of the computed data with the observation data. From these results together with Table 5, which shows that the total CPU and the number of timesteps do not show an increase for larger R_{xy} -values we can conclude that the use of bigger R_{xy} -values is better compared to smaller values.

From Table 7 it can be seen that the variance of the error in surface soil moisture decreases for increasing values of R_{xy} . This means that the error, which also itself decreases with increasing R_{xy} -values (table 6), is more smoothed over the grid cells. The decrease in variance between $R_{xy} = 50$ m and $R_{xy} = 250$ m is more than 20 percent.

Table 8: The effect of the different τ -values on the numerical and computational results.

| τ -values (G = 0.1, R = 100) | no-nudge | 900 | 1350 |
|-----------------------------------|----------------------|----------------------|----------------------|
| Cum. abs. mass bal. error | 1.64784 $\cdot 10^4$ | 1.46045 $\cdot 10^4$ | 1.56898 $\cdot 10^4$ |
| Cum. rel. mass bal. error | -5.70785 | -7.77830 | -8.83323 |
| Total back-stepping occur. | 1 | 3 | 0 |
| Total CPU for the simul. | 1408 | 1173 | 816 |
| Total timesteps | 9655 | 11294 | 7099 |
| Smallest timestep | 0.125 | 0.003906 | 0.0625 |
| Largest timestep | 32 | 32 | 32 |
| Average timestep | 1.491 | 1.275 | 2.028 |
| Avg NL iter. per timestep | 4.20 | 4.07 | 4.27 |
| τ -values (G = 0.1, R = 100) | 1800 | 2250 | 2700 |
| Cum. abs. mass bal. error | 1.57571 $\cdot 10^4$ | 1.53507 $\cdot 10^4$ | 1.52101 $\cdot 10^4$ |
| Cum. rel. mass bal. error | -9.10268 | -9.00813 | -9.04928 |
| Total back-stepping occur. | 10 | 11 | 0 |
| Total CPU for the simul. | 1040 | 1529 | 1564 |
| Total timesteps | 7196 | 11248 | 11284 |
| Smallest timestep | 0.0001221 | 0.0001221 | 0.0625 |
| Largest timestep | 32 | 32 | 32 |
| Average timestep | 2.001 | 1.280 | 1.276 |
| Avg NL iter. per timestep | 4.34 | 4.17 | 4.16 |

6.4 The influence of τ

The influence of the time during which the nudging technique is active (τ) has also been investigated. Table 8 shows the effect of the τ value on the numerical and computational results. From this table it can be seen that the cumulative relative mass balance error increases with increasing τ values and stabilizes for τ values of 1800 and higher around -9.05 percent. The number of back-stepping occurrences is generally small and even 0 for the runs with τ values equal to 1350 and 2700 s. The total CPU for the simulation reaches a minimum for τ equals 1350 of 816 seconds. For the runs with τ values of 2250 and 2700 this total CPU is almost twice as much compared to this minimum CPU. The total number of required timesteps shows a similar behavior with the exception of the high number of required timesteps for the run with τ equals 900 s. The smallest time step is relatively large for the nudge runs with τ values of 1350 and 2700 seconds but reaches the minimum allowed timestep for the runs with τ values 1800 and 2250 seconds. For all runs the timestep size reaches the maximum allowed 32 seconds. The largest average timestep size is reached for the two runs with τ values of 1350 and 1800 seconds, both with a value of over two seconds. The average nonlinear iterations is for all runs between 4.0 and 4.35.

Table 9 shows the influence of τ on the spatial error between the observed and computed soil moisture values at the surface nodes at three different times. At $t = 4200$ s, which is only 10 minutes after the first observation time, the mean difference increases with increasing τ -values. From this it seems that the spatial effect of the nudging technique close to the observation time is better for small values of τ . However the results for the two other times, which are both one hour away from the observation times, show the opposite behavior. The

Table 9: The influence of τ on the mean spatial difference of the soil moisture at the surface nodes between the base run and the nudging run at three different times (4200 s, 7200 s, 14400 s) for the atmospheric perturbation run.

| time | 4200 | 7200 | 14400 |
|---------------|--------|--------|--------|
| $\tau = 900$ | 0.2387 | 0.2172 | 0.1944 |
| $\tau = 1350$ | 0.2403 | 0.2038 | 0.1891 |
| $\tau = 1800$ | 0.2424 | 0.1975 | 0.1887 |
| $\tau = 2250$ | 0.2432 | 0.1919 | 0.1880 |
| $\tau = 2700$ | 0.2435 | 0.1874 | 0.1861 |

Table 10: The influence of τ on the variance (σ) of the differences between the base- and nudging run of the spatial soil moisture values at the surface nodes averaged over the whole simulation time.

| τ -value | σ |
|-----------------|----------|
| $\tau = 900$ s | 0.0244 |
| $\tau = 1350$ s | 0.0241 |
| $\tau = 1800$ s | 0.0238 |
| $\tau = 2250$ s | 0.0235 |
| $\tau = 2700$ s | 0.0235 |

difference between observed and computed data decreases with increasing τ -values. This is because the nudging technique is active longer for runs with higher τ -values than with small τ -values causing that at times not close to the observation times the error is smaller compared to the runs with small τ -values.

Table 10 shows the influence of τ on the variance of the spatial error of the surface soil moisture values and from this table it can be seen that the variance slightly linearly decreases with increasing τ till τ reaches the value of 2250 s. For higher values σ remains constant at a value of 0.0235, which is only 3.7 percent less than for τ of 900 s.

The influence of τ on the temporal variation of soil moisture values has also been investigated. Figure 17 shows the influence of τ on the temporal behavior of the soil moisture at the five nudging points. The thick line represents the observation data, and the dotted line the no nudging run. The nudging runs are labeled 1 to 5 representing the τ values ranging from 900 s to 2700 s. From the bottom three graphs it can clearly be seen that the shorter τ , the longer the nudging run follows the no nudging run. For the run with $\tau = 2700$ the results of the nudging run already differ from the no nudging run after 900 s, while the nudging effect for the run with $\tau = 900$ s can only be seen after 2700 seconds. Also after the first observation time at first the $\tau = 900$ run converges to the no nudging run, while the other runs remain longer close to the observed data. This convergence towards the no nudge run is much stronger for the runs with low τ -values compared to the runs with higher τ values as a results of the smaller influence time of the nudging technique. This same behavior can also be seen for the second observation time but the differences between the nudging runs are much smaller at this time.

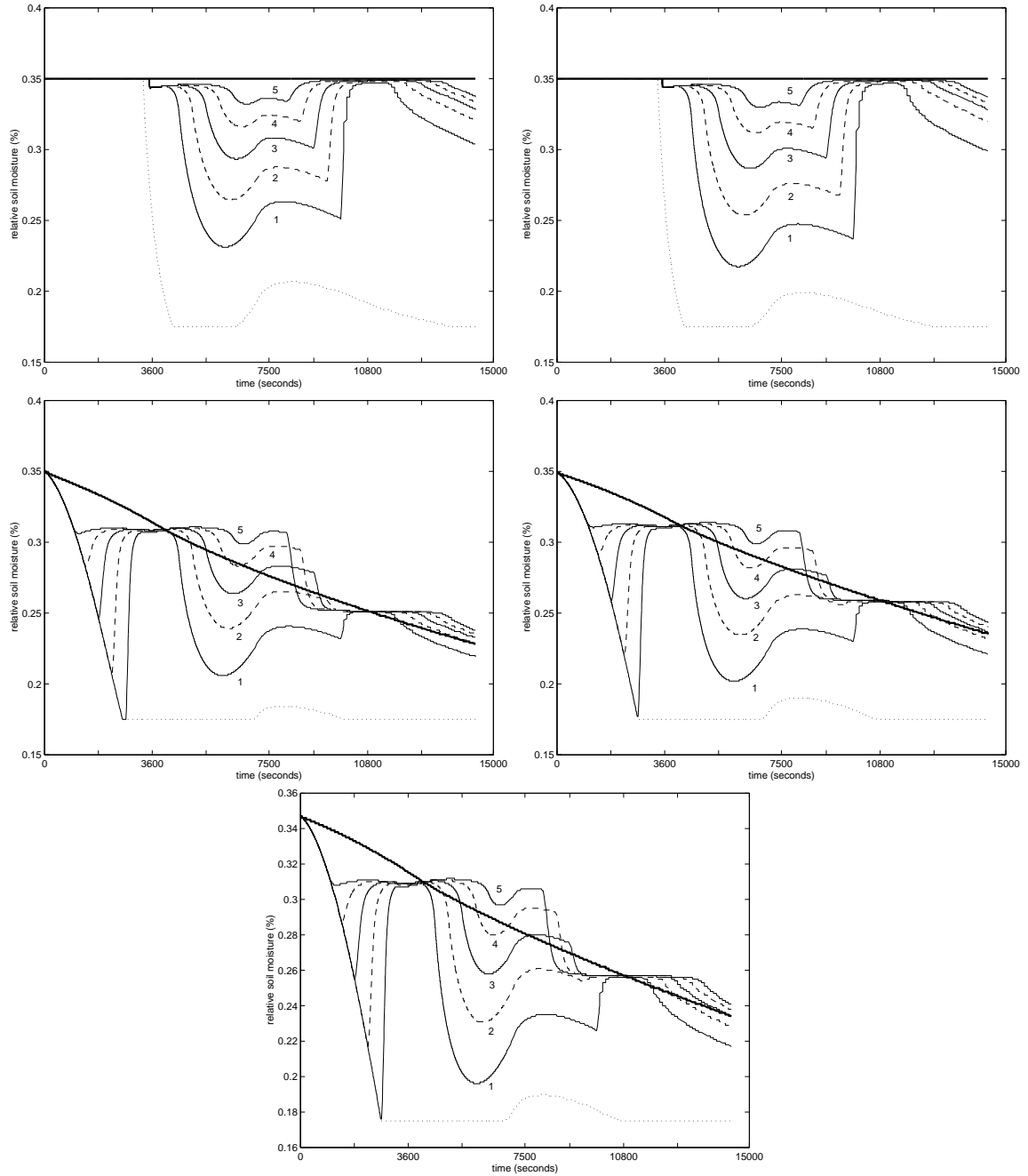


Figure 17: The influence of τ on the temporal behavior of the soil moisture content at the five nudging points together with the base run (thick line) and the no nudging run (dotted line). 1: $\tau = 900s$, 2: $\tau = 1350s$, 3: $\tau = 1800s$, 4: $\tau = 2250s$, 5: $\tau = 2700s$

From these three plots the influence of the weighting functions can clearly be seen. The temporal dependency of the weighting functions has been defined as a head function (see Figure 3). This weighting function increases over a time period of $\tau/2$ linearly from 0 to 1 and remains 1 for a period of τ after which it decreases linearly to 0 over a time period of $\tau/2$. The period when the weighting function remains 1 can be recognized in the convergence of the nudging runs to the base run. From these three plots it can be seen that the nudge run does not converge to the actual value of the base run at the start of the assimilation time but converges until it reaches the value observed at the first observation time and remains constant, as a result of the defined temporal dependency of the weighting function for a period of τ .

From the upper two graphs it can be seen that the defined time of nudging influence implies that the nudge runs with larger τ values remain close to the observed saturated soil moisture values for a longer time, while the runs with lower τ values converge quicker, longer and therefore further toward the no nudging run for both assimilation times.

From the three bottom plots it can be concluded that higher τ values do not necessarily lead to better results in the temporal behavior of soil moisture values. The run with τ value equal to 2700 overestimates the base run much more compared to the runs with $\tau = 1800$ and $\tau = 2250$, which seem to have a better agreement with the base run between the two assimilation times.

For the upper two graphs however higher τ values do lead to a better agreement with the base run, because overestimating is in this particular case (saturated observed data) not possible. Generally however it can be concluded that a longer time of influence does not for all cases lead to better results in the temporal behavior of soil moisture. However for very small values of τ the results are worse than for very high values from which can be concluded that it is preferable to take higher τ values.

7 Conclusions and recommendations

7.1 Conclusions

From the application of the CATHY model to the testcase it can be concluded that the implementation of the nudging technique has a positive influence on the hydrological results. Especially for the grid cells in which the five defined nudging points are located and the surrounding cells, the computed results of the nudging run show a better agreement with the observed values than the run without the nudging technique. This improvement is strongest during the assimilation times, but also at the end of the simulation, which is one hour after the last observation time and half an hour after the last assimilation time has ended, a clear improvement compared to the run without the nudging technique can still be seen.

This improvement is made because during the assimilation times the computed hydrological variables at and around the nudging points are driven towards the observed data to reach a better agreement with these values. However for the atmospheric perturbation run an immediate increase in difference between the observed and computed data is noticed after the assimilation time has ended, while for the initial condition perturbation run the computed values remain close to the observed values, also after the assimilation time has ended.

From these two perturbation runs it is difficult to draw general conclusions regarding the effect of the nudging technique on the computation time. In this case the run including the nudging technique is more efficient for the atmospheric perturbation run, while for the initial conditions perturbation run the run without the nudging technique shows a better computational efficiency.

Besides this general effect of the nudging technique on the results also the influence of three separate nudging parameters has been determined. The influence of G on the nudging effect is that generally for increasing G values a decrease in the mean areal difference between observed and computed data is reached. This improvement is not only made during the assimilation times but also after the nudging technique is not active anymore. The improvement in the spatially computed data is reached because for larger G values the computed data converge stronger towards the observation data during assimilation times and reach therefore a better agreement with these values. However for G values larger than 0.1 almost no difference in convergence can be noticed. This is also the reason why the decrease in mean spatial error stabilizes for G values larger than 0.1.

From this stabilization in improvement of the hydrological results, together with the fact that for higher G values, especially for those of 0.5 and higher, the number of back-stepping occurrences and therefore the total number of required time steps increase rapidly causing a much higher total CPU compared to smaller G values, it can be concluded that it is not recommendable to take high G -values. In this case an optimal value of G is between 0.05 and 0.1.

In contrast to increasing G values, increasing values of R_{xy} do not lead to an increase in back-stepping occurrences and total number of timesteps and therefore do not show an increase in total CPU. The minima for these variables are even reached for a run with a relative high value of R_{xy} . Increasing R_{xy} values lead to considerable decreases in the mean spatial differences between the observed and computed values. This is because a larger area around the observation points is influenced by the nudging technique when using higher R_{xy} values. Also the variance of the spatially distributed error decreases with increasing R_{xy} values, showing that for a larger radius of influence not only the mean error is smaller but also that the error is more smoothed over the grid cells. In contrast to increasing G values, the improvements in the mean spatial error do not stabilize for high R_{xy} values. The influence of R_{xy} on the convergence towards the observed data at the nudging points is much smaller compared to the influence of G and τ on this convergence.

From these improvements for higher R_{xy} values without requiring more CPU it can therefore be concluded that it is better to take high values for the horizontal radius of nudging influence.

From the investigations of the influence of the time of the nudging technique being active it can be concluded the mean spatial error decreases with increasing τ values at times outside the assimilation period, while the spatial error increases with increasing τ values at times close to the observation times. It seems that the smaller τ , the stronger the influence of the nudging technique is during the assimilation time, while due to the small time of nudging influence, its influence further away from the observation times decreases. Further it can be concluded that for higher τ values the convergence toward the observation values is stronger and lasts longer. However higher τ values do not necessary lead to better results, because for high τ values the computed results between the two assimilation times could remain too long at the value of the first observed value while the actual observed values change. Therefore it can be concluded that a higher time of nudging influence does not automatically lead to

better results.

7.2 Recommendations

This study was a first testing of a data assimilation technique (Newtonian relaxation), implemented in a complex spatially distributed hydrological model, to one particular testcase. This study provides a first impression of the influence of the nudging technique on the hydrological and numerical results. However to get a better understanding of the the exact influence of the nudging technique and its parameters, further research is required. Therefore a few recommendations for further research are summarized in this paragraph.

The influence of the number of observation times and therefore assimilation periods needs still to be investigated. Because small τ values seem to have a better agreement with the observed data close to the observation times but perform worse further away from these observation times it would be interesting to see the effect of more assimilation times with smaller τ values on the results.

Because the influence of the nudging parameters has only been investigated for one particular test case it would also be good to see the effect of these parameters in other testcases in order to draw general conclusions. For example, is the same optimal value of G reached? Does the improvement of the hydrological results always stabilize for high G values? Does increasing the radius of influence always lead to better results without requiring a higher CPU?

Finally, to get a better understanding of the nudging technique more research has to be done on the influence of the weighting functions (W). Are the defined functions for the horizontal, vertical and temporal dependency the optimal ones? What would be the effect on the influence of the nudging technique if the defined “head function” for the temporal influence is replaced by one similar to that used for the horizontal influence?

Acknowledgments This work has been supported in part by the European Commission (contract EVK1-CT-1999-00022), by the Italian Ministry of the University (project ISR8, C11-B), and by the Sardinia Regional Authorities.

References

- Bixio, A. C., S. Orlandini, C. Paniconi and M. Putti, Physically-based distributed model for coupled surface runoff and subsurface flow simulation at the catchment scale. In: Bentley, L. R. (ed.) *Computational Methods in Water Resources, Vol. 2*. Balkema, Rotterdam, The Netherlands, pp 1115–1122, 2000.
- Brooks, R. H. and A. T. Corey, Hydraulic properties of porous media. Hydrology Paper 3, Colorado State University, Fort Collins, CO, 1964.
- Daley, R., *Atmospheric Data Analysis*. Cambridge University Press, Cambridge, UK, 1991.

- Houser, P. R., W. J. Shuttleworth, J. S. Famiglietti, H. V. Gupta, K. H. Syed and D. C. Goodrich, Integration of soil moisture remote sensing and hydrologic modeling using data assimilation, *Water Resour. Res.* 34(12), 3405–3420, 1998.
- Huyakorn, P. S., S. D. Thomas and B. M. Thompson, Techniques for making finite elements competitive in modeling flow in variably saturated porous media, *Water Resour. Res.* 20(8), 1099–1115, 1984.
- Marrocu, M. and C. Paniconi, Assessment and formulation of data assimilation techniques for a 3D Richards equation-based hydrological model. Technical Report CRS4-TECH-REP-01/73, Center for Advanced Studies, Research and Development in Sardinia, Cagliari, Italy, 2001.
- McLaughlin, D., Recent developments in hydrologic data assimilation. In: Pielke Sr., R. A. and R. M. Vogel (eds.) *U.S. National Report to International Union of Geodesy and Geophysics 1991–1994: Contributions in Hydrology 977–984*, American Geophysical Union, Washington, DC, 1995.
- Montgomery, D. R. and E. Foufoula, Channel network source representation using digital elevation models, *Water Resour. Res.* 29(12), 3925–3934, 1993.
- Orlandini, S. and R. Rosso, Diffusion wave modeling of distributed catchment dynamics, *J. Hydrol. Engrg., ASCE* 1(3), 103–113, 1996.
- Paniconi, C. and E. F. Wood, A detailed model for simulation of catchment scale subsurface hydrologic processes, *Water Resour. Res.* 29(6), 1601–1620, 1993.
- Paniconi, C., M. Marrocu, M. Putti and M. Verbunt, Newtonian nudging for a Richards equation-based finite element model of coupled overland and subsurface flow, *Adv. Water Resour.* , 2001 (in preparation).
- Putti, M. and C. Paniconi, A catchment model of coupled surface and subsurface flow, *Water Resour. Res.* , 2001 (in preparation).
- van Genuchten, M. T. and D. R. Nielsen, On describing and predicting the hydraulic properties of unsaturated soils, *Ann. Geophys.* 3(5), 615–628, 1985.